NRL Report 7498

# Design and Applications of a Holographic System for Crystal-Growth Studies

J. A. BLODGETT

*Applied Optics Branch*
*Optical Sciences Division*

and

R. J. SCHAEFER

*Transformations and Kinetics Branch*
*Metallurgy Division*

January 2, 1973

**NAVAL RESEARCH LABORATORY**
**Washington, D.C.**

Approved for public release; distribution unlimited.

## CONTENTS

Abstract ..... 1
Problem Status ..... 1
Authorization ..... 1

FOREWORD ..... 1

INTRODUCTION ..... 2

PRINCIPLES OF HOLOGRAPHIC IMAGING ..... 3

HOLOGRAPHIC MICROSCOPY ..... 11

- Modified Conventional Microscope ..... 12
- Intermediate-Lens Technique ..... 13
- High-Resolution Direct Holographic Recording ..... 15

INTERFEROMETRIC TECHNIQUES ..... 16

EXPERIMENTAL SYSTEMS ..... 20

- Laser ..... 20
- Table ..... 21
- Optical Components ..... 22
- Film ..... 23
- Sample-Growth Chambers ..... 24
- Reconstruction Techniques ..... 26
- Photomicrography ..... 26

APPLICATIONS TO CRYSTAL-GROWTH STUDIES ..... 27

- Planar Interfaces ..... 27
- Dendrites ..... 31
- Freely Floating Crystals ..... 35
- Liquid Inclusions ..... 37

SUMMARY ..... 40

REFERENCES ..... 41

# Design and Applications of A Holographic System for Crystal-Growth Studies

J. A. BLODGETT

*Applied Optics Branch*
*Optical Sciences Division*

and

R. J. SCHAEFER

*Transformations and Kinetics Branch*
*Metallurgy Division*

Abstract: Holography, with its unique depth of field and interferometric capabilities, is a powerful new tool for the study of crystal growth. This report describes the theory and practice of forming and reconstructing holograms as applied to the study of microscopic phenomena. It outlines the technical considerations involved in the design of a holographic laboratory and describes the type of experimental results which may be obtained. A holographic laboratory could employ several techniques of holographic microscopy, including holographic interferometry. In the holographic work at NRL an argon ion laser was used to record holograms of transparent organic analogs to solidifying metals. Special observation chambers were constructed to allow holographic recording of planar solid/liquid interfaces, dendrites, floating crystals, and liquid inclusions in crystals. Crystal morphologies were measured by interferometric analysis of the reconstructed holograms. Crystal imperfections were shown to initiate surface relief features. A 2-percent anisotropy of the solid/liquid surface energy was found to control anisotropic crystal growth.

## FOREWORD

This report describes the use of holography for a study of crystal growth. In includes discussions of basic holographic principles, specific techniques for holographic microscopy, and application of these techniques to crystal-growth research. The primary objective of the report is to outline the technical considerations involved in the design of a holographic laboratory and describe the type of experimental results which may be obtained. These may be useful to readers planning to initiate holographic studies of crystal growth and other microscopic phenomena.

NRL Problems N01-16-101 and M01-23-101; Projects RR 011-07-41-4807 and RR 022-01-46-5430. This is a summary report on a continuing project. Manuscript submitted October 6, 1972.

## INTRODUCTION

Holography is a process which records and reconstructs images of objects illuminated by coherent light. Invented by Gabor in 1948 [1-3], holography became practical only with the development of lasers in the early 1960's. Reconstructed images of high quality became possible when Leith and Upatnieks [4-6] introduced techniques for separating the overlapping images which caused confusion in Gabor's original method. A multitude of special techniques have since been suggested or demonstrated for improving the quality of holographic images and for extracting information from the images. Similarly, many applications of holography to research, testing, and various forms of information storage and processing have been demonstrated or suggested. The number of cases in which holography has actually been used as a working tool, however, has been relatively limited.

To record a hologram of an object by the basic technique of Leith and Upatnieks, a beam of coherent monochromatic light is split into two beams. One beam illuminates the object, and light from the object then falls on a photosensitive medium. The other beam travels by a separate path bypassing the object and falls on the same area of the photosensitive medium. The interference pattern generated by the overlapping object and reference beams is recorded to form the hologram. When this hologram is illuminated, it acts as a diffraction grating to reconstruct an image of the original object.

The image reconstructed from a hologram has certain special properties which make it quite different from conventional photographs. The holographic image, real or virtual, exhibits a three-dimensional character complete with parallax effects. All points in the image, regardless of their distance from the hologram plane, are reconstructed in sharp focus. Of greatest significance for technical applications is that the hologram reconstructs the phase, as well as the amplitude, of the light originally coming from the object. These special properties of holographic images can be extremely useful for recording events occurring throughout the volume of an experimental test chamber, especially because interferometric techniques can be used for precise measurements of the recorded objects. Holography is thus well suited for studies of crystal growth.

Holography as an experimental tool does have some basic disadvantages which the worker must be prepared to accept. One troublesome effect is speckle, a harsh granularity, characteristic of images formed by coherent light, which tends to obscure the useful information in the image. Because of the speckle, images reconstructed from holograms generally appear much more grainy than images of comparable resolution formed by incoherent light.

Making and reconstructing holograms generally involves significantly more labor than making and viewing conventional photomicrographs. Commercial units which make holography as easy as conventional photomicrography are now becoming available, but such units have less versatility than systems composed of individual movable components. In either case the cost of holographic apparatus can be expected to remain relatively high.

Holography is justified only when one plans to take advantage of the special properties of holographic images. In situations where one wishes to observe events occurring at unpredictable locations, or where one wishes to measure precisely complex changes of shape, no other technique can compare with holography.

The general theory of holography is described in detail in several books [7-12]. The purpose of this report is to describe the use of holography specifically in the study of microscopic phenomena.

## PRINCIPLES OF HOLOGRAHIC IMAGING

The following discussion of the general requirements for holographic imaging will convey a better understanding and appreciation of the system design features affecting the information content of the reconstructed image, including limitations on field of view and resolution. The discussion will be limited to the off-axis type of hologram initially described by Leith and Upatnieks [4-6], since the off-axis type seems best suited for holographic microscopy. In addition, only plane holograms as distinct from volume holograms will be considered. A volume hologram is one in which the thickness of the recording medium is greater than the spacing of the fringes formed by the interference of the reference and object waves at the recording plane. The thickness of photographic emulsions is generally 5 $\mu$m or greater; therefore holograms formed in visible light ($\lambda \approx 0.5$ $\mu$m) are volume holograms when the angle between the object and reference waves is greater than approximately 6°. Although most holograms are actually volume holograms, the restriction to plane holograms will simplify the discussion and in most cases will provide a good first approximation to the theory of the primary effects.

To understand the theory of holographic techniques for recording and reconstructing images, we consider an isotropic dielectric medium and the case of linearly polarized, monochromatic waves. The light disturbance at a point $\vec{x}$ and time $t$ can be represented by a scalar function $u(\vec{x},t)$, where

$$u(\vec{x},t) = U(\vec{x}) \cos[2\pi f t + \phi(\vec{x})], \tag{1}$$

in which $U(\vec{x})$ and $\phi(\vec{x})$ are the amplitude and phase at the point $\vec{x}$ and $f$ is the frequency of the monochromatic wave. Complex notation will be employed, so that $u(\vec{x},t)$ may be written

$$u(\vec{x},t) = \mathrm{Re}[\underset{\sim}{U}(\vec{x}) \exp(-j2\pi f t)] \tag{2}$$

where

$$\underset{\sim}{U}(\vec{x}) = U(\vec{x}) \exp[-j\phi(\vec{x})]. \tag{3}$$

With reference to Fig. 1 the object wave at the recording plane may be written

$$\underset{\sim}{o}(x,y) = o(x,y) \exp[-j\phi(x,y)] \tag{4}$$

and the reference wave

$$\underset{\sim}{r}(x,y) = r(x,y) \exp[-j\Psi(x,y)]. \tag{5}$$

Any detector employed in the recording plane will respond only to the intensity of the incident light waves, given by

$$\begin{aligned} I(x,y) &= |\underset{\sim}{o}(x,y) + \underset{\sim}{r}(x,y)|^2 \\ &= |\underset{\sim}{o}(x,y)|^2 + |\underset{\sim}{r}(x,y)|^2 + 2o(x,y)r(x,y) \cos[\phi(x,y) - \psi(x,y)]. \end{aligned} \tag{6}$$

The last term in Eq. 6 depends on the relative phase of the object and reference waves at a given point in the recording plane; thus both the amplitude and phase of the object wave are recorded in holography.

We will assume that a photographic emulsion is placed in the recording plane and that this emulsion is exposed and processed such that its amplitude transmission after processing is

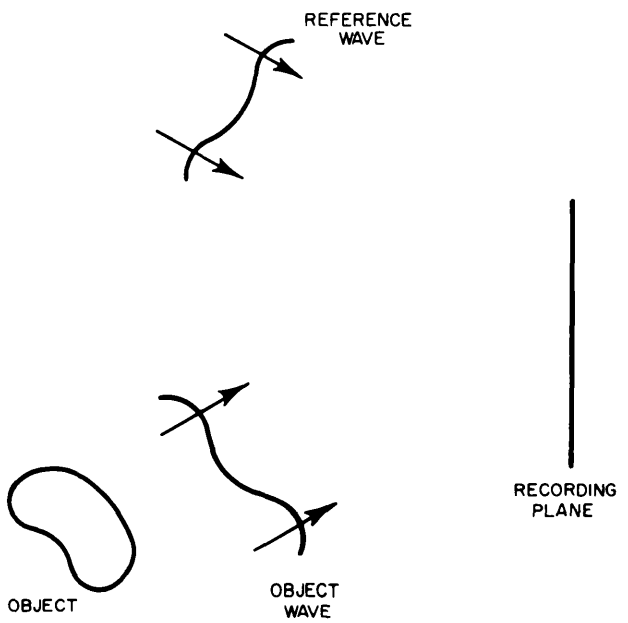


Fig. 1 – A general arrangement for recording a hologram with an off-axis reference wave

a linear function of the exposure. A typical relation between amplitude transmission and exposure for a photographic emulsion is shown in Fig. 2. If the intensity of the reference wave $|\underset{\sim}{r}|^2$ is uniform across the recording plane, then the amplitude transmittance $T_A$ may be written

$$T_A(x,y) = T_r + \beta\Delta t(|\underset{\sim}{o}|^2 + \underset{\sim}{o}^*\underset{\sim}{r} + \underset{\sim}{o}\,\underset{\sim}{r}^*), \tag{7}$$

where $T_r$ is the transmittance due to the reference wave alone, $\beta$ is the slope of the $|T_A|$ versus $E$ curve in the linear range, $\Delta t$ is the exposure time, and the asterisk indicates the complex conjugate. This relationship is valid provided that the variation of the object wave across the detector plane is small compared to the amplitude of the reference wave and that the exposure lies within the linear range of the $|T_A|$ versus $E$ curve.

To reconstruct the recorded object wave, the processed hologram is illuminated by another beam $\underset{\sim}{R}(x,y)$. The wave transmitted by the hologram is then

$$\underset{\sim}{R}(x,y)T_A(x,y) = \underset{\sim}{R}(x,y)T_r + \beta\Delta t[|\underset{\sim}{o}|^2\underset{\sim}{R} + \underset{\sim}{o}^*\underset{\sim}{r}\underset{\sim}{R} + \underset{\sim}{o}\,\underset{\sim}{r}^*\underset{\sim}{R}]. \tag{8}$$

If the reconstruction wave duplicates the reference wave, namely,

$$\underset{\sim}{R}(x,y) = \underset{\sim}{r}(x,y), \tag{9}$$

then the transmitted wave is given by

$$\underset{\sim}{r}(x,y)T_A(x,y) = \underset{\sim}{r}(x,y)T_r + \beta\Delta t|\underset{\sim}{o}|^2\underset{\sim}{r} + \beta\Delta t\,\underset{\sim}{o}^*\underset{\sim}{r}^2 + \beta\Delta t\,\underset{\sim}{o}|\underset{\sim}{r}|^2. \tag{10}$$

If, as was previously assumed, $|\underset{\sim}{r}|^2$ is uniform, then the fourth term on the right in Eq. 10 is an exact duplication of the original object wave. To an observer this wave appears to be diverging from the original object even though the object may no longer be present; therefore, a virtual

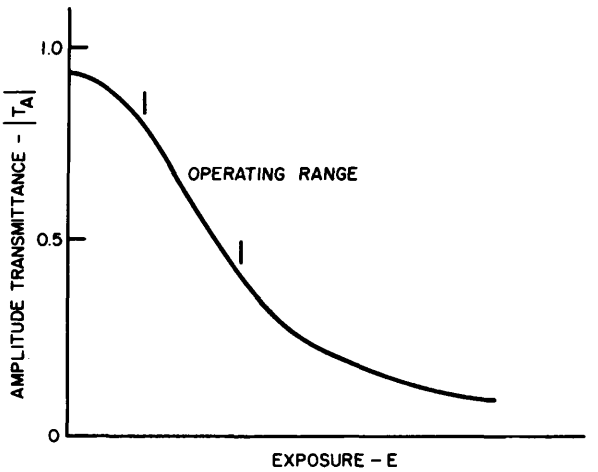


Fig. 2 — Relation between transmittance and exposure for a typical holographic emulsion

image of the object is created. If instead the reconstruction wave is chosen to be the conjugate of the reference wave, then the third term on the right is seen to be proportional to the complex conjugate of the object wavefront $\beta\Delta t|\underset{\sim}{r}|^2\underset{\sim}{o}^*$. This generally results in a converging wavefront which forms a real image in space. This real image is the complex conjugate of the object wave. The intensity of the image is not affected, but the phase is changed.

The holographic process therefore records the object wavefront completely, permitting at a later time the reconstruction of the object field. This reconstructed wavefront has properties identical to the original wavefront from the physical object. The one remaining problem is the separation of the various terms on the right side of Eq. 10 from the term of interest, and this is readily accomplished by the off-axis holographic technique of Leith and Upatnieks [4-6].

One arrangement for recording an off-axis hologram is shown in Fig. 3. In this instance the reference is a plane wave incident at an angle $\theta$ to the holographic emulsion and the object wave considered comes from one single point on the object located at coordinates $(x_0, y_0, z_0)$. The quadratic approximation for spherical waves will be used. At the emulsion the amplitude distribution may be written

$$V(x,y) = r\exp(-j\frac{2\pi}{\lambda}x\sin\theta) + o\exp\left\{j\frac{\pi}{\lambda z_0}[(x-x_0)^2 + (y-y_0)^2]\right\}. \tag{11}$$

If we again assume that the amplitude transmission of the processed hologram is proportional to the exposures as in Eq. 7, then

$$\begin{aligned} T_A(x,y) = T_r + \beta\Delta t\Big(o^2 + ro\exp\left\{j\frac{2\pi}{\lambda}x\sin\theta + j\frac{\pi}{\lambda z_0}[(x-x_0)^2 + (y-y_0)^2]\right\} \\ + ro\exp\left\{-j\frac{2\pi}{\lambda}x\sin\theta - j\frac{\pi}{\lambda z_0}[(x-x_0)^2 + (y-y_0)^2]\right\}\Big). \end{aligned} \tag{12}$$

Illuminating this hologram with a duplicate of the reference wave gives the following three terms:

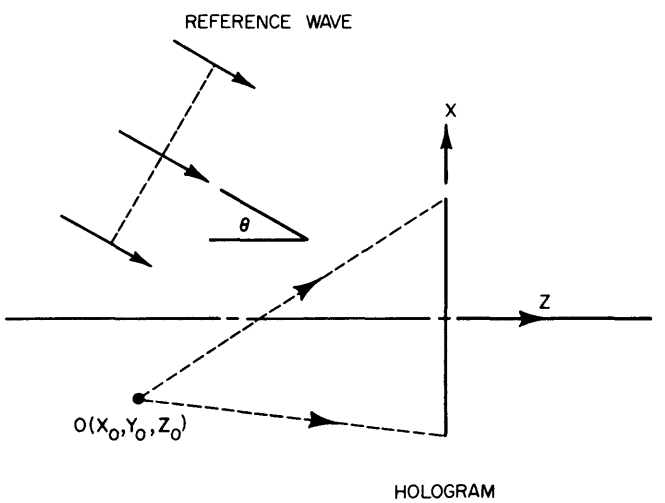


Fig. 3 – An arrangement for recording holograms employing a plane off-axis reference wave and a simple spherical object wave.

$$u_1 = [T_r + \beta\Delta t o^2] r \exp\left(-j\frac{2\pi}{\lambda}x \sin\theta\right), \tag{13a}$$

$$u_2 = \beta\Delta t\ r^2 o \exp\left\{+j\frac{\pi}{\lambda z_0}[(x - x_0)^2 + (y - y_0)^2]\right\}, \tag{13b}$$

$$u_3 = \beta\Delta t\ r^2 o \exp\left\{-j\frac{\pi}{\lambda z_0}[(x - x_0)^2 + (y - y_0)^2]\right\} \exp\left(-j\frac{4\pi}{\lambda}x \sin\theta\right). \tag{13c}$$

The first term is a transmitted wave propagating in the direction of the reconstruction beam. The second term is a diffracted wave which reconstructs a virtual image of the object in its original position. The third term is a diffracted wave which reconstructs a real image of the object but at coordinates $(x_0 - 2z_0 \sin\theta,\ y_0,\ -z_0)$ as seen in Fig. 4a. This technique has therefore permitted a spatial separation of the three terms in the reconstruction process; and the virtual image can be viewed without any disturbing background caused by the other terms. Had the reconstruction wave been the complex conjugate of the original reference wave, as shown in Fig. 4b, then a real image of the point source would have been formed at coordinates $(x_0,\ y_0,\ z_0)$.

If a hologram had been formed with two object points, the reconstructed virtual image would be as in Fig. 5a. A complete three-dimensional reconstruction of the object can be viewed with all the parallax effects present with the original object. When the real image is viewed as in Fig. 5b, however, the point which was originally closest to the observer and hologram plane is now still closest to the hologram plane but farthest from the observer. The parallax relations are not the same as those in the original scene. This generally causes no difficulties in crystal growth studies, but it can cause difficulties with more complicated three-dimensional objects.

The separation of the real and virtual images in the reconstruction depends on the angular offset of the reference wave. For no overlap this angle must be greater than a certain minimum which will be discussed later. The angular offset of the reconstruction wave is assumed to be the same as that of the reference wave. If the reconstruction wave is incident at a different angle on the idealized plane hologram considered here, the real and virtual images would still have been reconstructed properly; but they would have occurred at different positions. When the

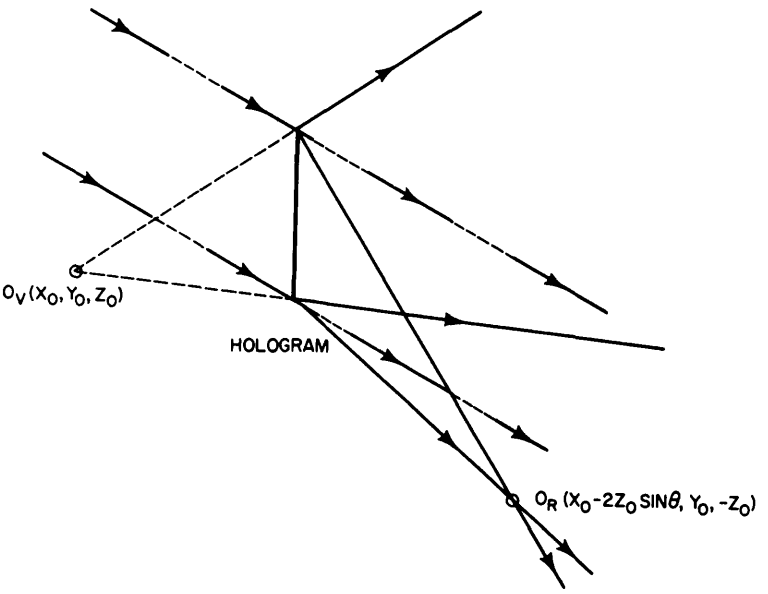


(a) Reconstructed with a duplicate of the original reference wave

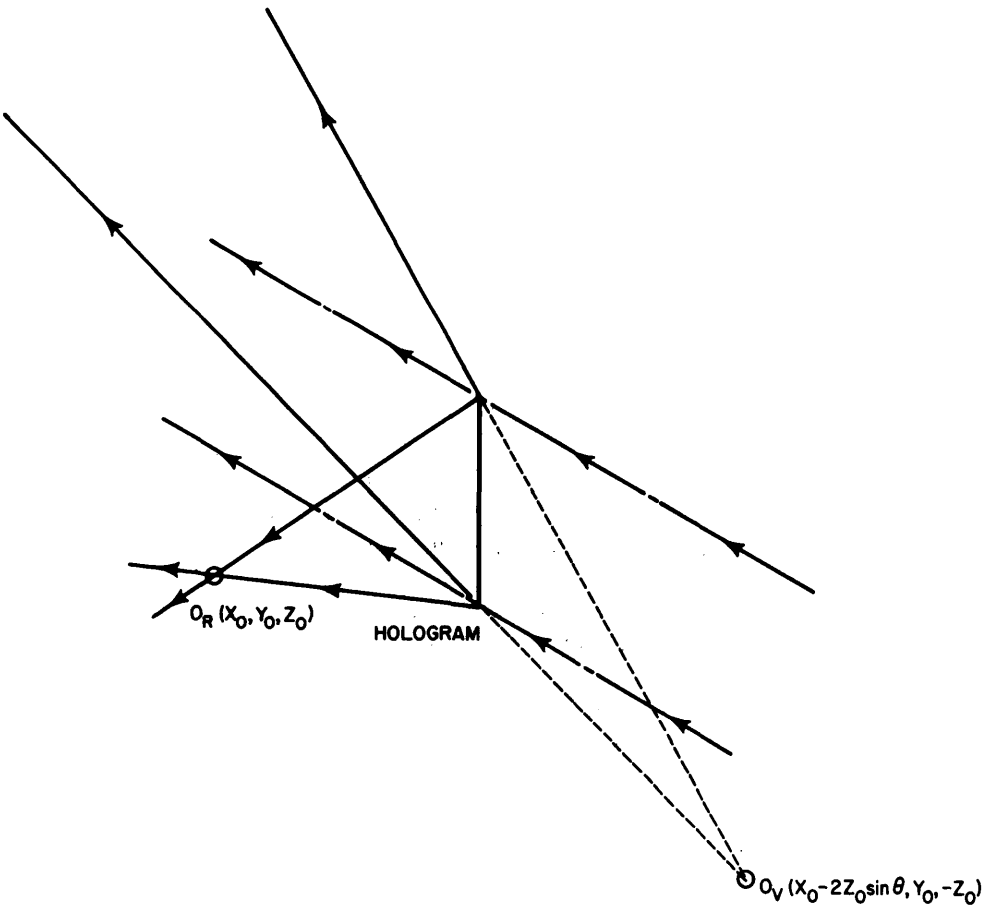


(b) Reconstructed with the complex conjugate of the reference wave

Fig. 4 — Reconstruction from the hologram as recorded in Fig. 3

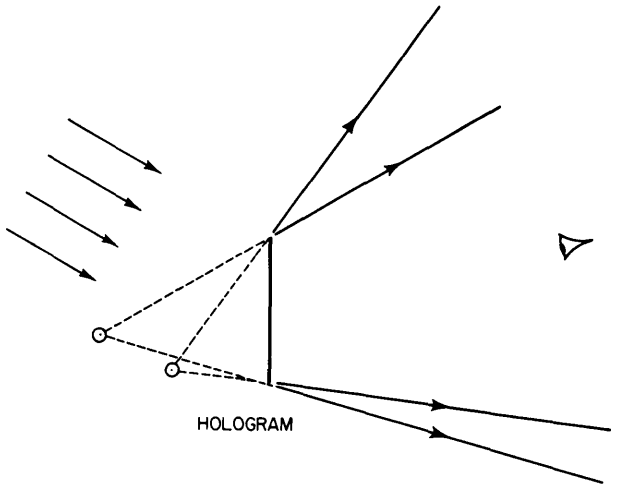


(a) Virtual images of the two object points seen in their original relative positions with the three-dimensional character retained

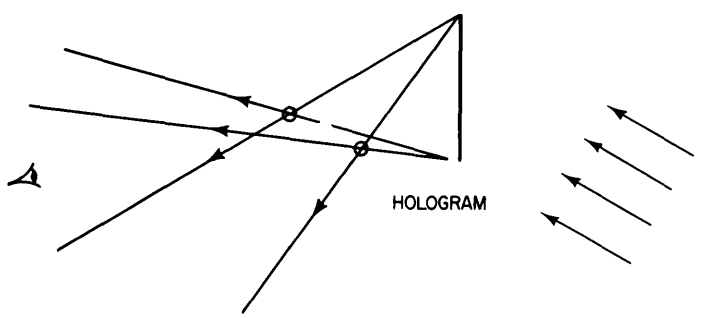


(b) Relative positions of the two points inverted

Fig. 5 – Reconstruction from a hologram recorded with two object points

thickness of the emulsion is taken into account, however, the reference wave must be duplicated exactly to obtain an undistorted virtual image. Similarly, the exact conjugate of the reference wave must be used to obtain an undistorted real image.

There is nothing particularly unique about the use of a plane reference wave. Any wavefront that can be reproduced for reconstruction, a diverging spherical wave for example, could be used when only the virtual image is of interest. When the reconstructed real image is of interest, however, the conjugate of the reference wave must be available. If a diverging spherical reference wave is employed, then its conjugate, a converging spherical wave, is required. The conjugate of a plane wave is another plane wave; therefore this is the simplest wavefront to use as a reference when the real image is of interest.

When the reference and reconstruction waves are not identical (or conjugates), a reconstructed image will still be formed, but magnification and aberrations will be found in this image. The same is true if the wavelengths of the reference and reconstruction waves are different [13,14].

To determine the minimum offset angle for the reference wave to avoid spatial overlap of the various terms in the reconstruction (Eq. 10), it is advantageous to consider the spatial bandwidths involved. The interference fringes found in the hologram plane are due to interference between various points on the object and the reference wave and between various points on the object itself. With reference to Fig. 6 the maximum fringe frequency at the center of the hologram plane due to interference between two points on an object of angular extent $\phi$ is given by

$$\nu_{\substack{o-o \\ \max}} = \frac{2}{\lambda} \sin \frac{\phi}{2}. \tag{14}$$

This fringe structure is represented in Eq. 10 by the term proportional to $|\underset{\sim}{o}|^2$. If a plane wave is incident on a grating with a spatial frequency equal to $\nu_{\substack{o-o \\ \max}}$, then the first-order diffracted beams will be at angles $\alpha$ given by

$$\sin \alpha = 2 \sin \frac{\phi}{2}. \tag{15}$$

Thus the interference structure found on the hologram due to the term in $|\underset{\sim}{o}|^2$ diffracts light into an angle $2\alpha$, $\alpha$ being given by Eq. 15. To avoid overlap between the terms proportional to $\underset{\sim}{o}$ and the term proportional to $\underset{\sim}{o}^*$, the minimum fringe frequency formed by interference between a point on the object and the reference wave $\nu_{\substack{o-r \\ \min}}$ must be greater than $\nu_{\substack{o-o \\ \max}}$. From Fig. 6

$$\nu_{\substack{o-r \\ \min}} = \frac{\sin \theta - \sin \frac{\phi}{2}}{\lambda}. \tag{16}$$

Equating $\nu_{\substack{o-r \\ \min}}$ and $\nu_{\substack{o-o \\ \max}}$ gives

$$\sin \theta = 3 \sin \frac{\phi}{2} \tag{17}$$

For the case in which the reference wave is much stronger than the object wave this condition can be relaxed, since the terms proportional to $\underset{\sim}{o}$ and $\underset{\sim}{o}^*$ will be much stronger than the term proportional to $|\underset{\sim}{o}|^2$. Then all that is required is for

$$\sin \theta \geqslant \sin \frac{\phi}{2}. \tag{18}$$

as this will be sufficient to separate the real and virtual images.

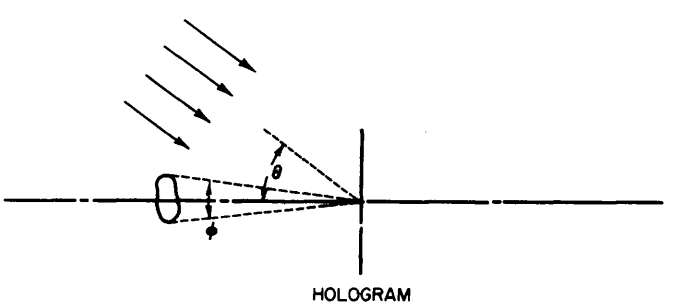


Fig. 6 – Hologram recording arrangement showing the notation used in calculating the spatial frequencies of the fringes due to the object and reference waves

To record the hologram, a photosensitive medium is required having sufficient resolution to record the fringes formed by the interference of the object and reference waves. Several materials have been successfully used; however, a photographic emulsion is the most sensitive material with adequate resolution. For a reference wave making an angle of approximately 45° with the object wave, the interference fringes formed at the hologram have a spatial frequency of almost 1400 cycles/mm for a wavelength $\lambda$ of 0.5 $\mu$m. Therefore only very-high-resolution emulsions are suitable for recording off-axis holograms. These emulsions are relatively insensitive compared to conventional photographic films and plates.

The fringes recorded in a photographic emulsion form an amplitude diffraction grating. Since the efficiency of this grating (the ratio of the intensity of the diffracted light to the intensity of the incident light) is proportional to the square of the visibility of the fringes, it is important that the emulsion have sufficient resolution. Fringe visibility as used here is given by

$$V = (I_{max} - I_{min})/(I_{max} + I_{min}). \tag{19}$$

The diffraction efficiency as a function of the spatial frequency of the grating recorded is plotted for a typical holographic emulsion in Fig. 7. The maximum diffraction efficiency for this type of grating is limited to a few percent [15]. This can cause difficulties in examining the reconstructed image, since adequate intensity may not be available. The diffraction efficiency of these holographic gratings can be greatly increased by bleaching the holograms to form phase gratings. The holograms must be bleached carefully, however, to avoid introducing noise in the reconstructed image [16,17].

The suitability of a light source for the production and reconstruction of holograms is directly related to its coherence properties. We assumed a monochromatic source in the analysis of the

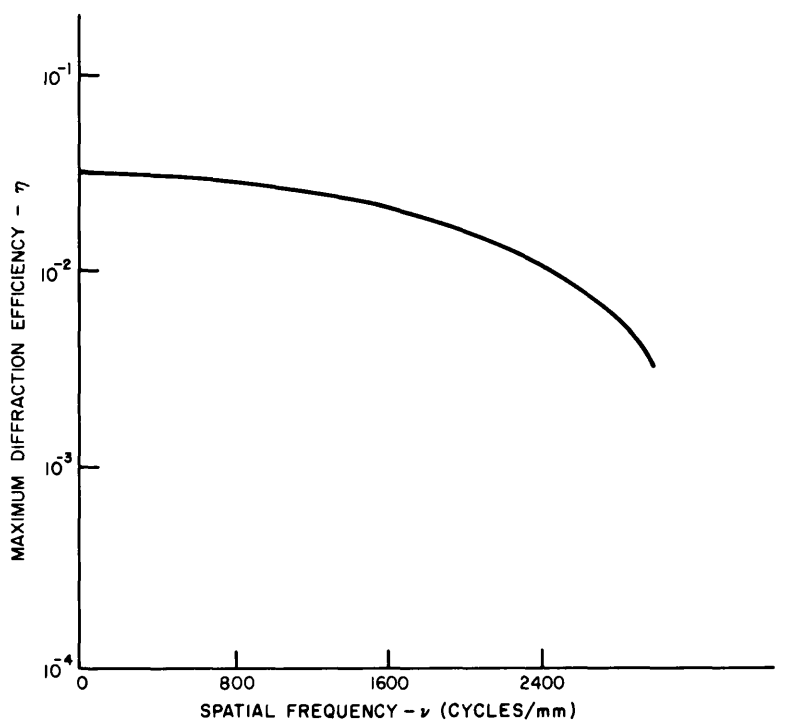


Fig. 7 – Diffraction efficiency versus spatial frequency for a typical holographic emulsion

formation and reconstruction of the holograms. No source is truly monochromatic; however the spectral bandwidth of many lasers is extremely narrow, less than 0.1 Å. The coherence length for ion lasers, which is directly related to the spectral bandwidth, is typically of the order of 10 cm; and the use of an intracavity etalon can increase this to several meters. In addition these lasers can be operated in the lowest order transverse mode, $TEM_{00}$, so that there are no problems associated with poor transverse coherence. Various portions of the wavefront can interfere with one another. The visibility of the fringes formed at the hologram, which is a function of coherence length assuming good transverse coherence, is therefore not significantly limited by the sources available. Even when a pulsed laser is required, a $Q$-switched ruby system can be constructed which has an output pulse with a coherence length of greater than 1 meter and which operates in the $TEM_{00}$ mode. Other laser sources are available and occasionally used in holography; however for the type of system described in this report the ion laser, the He-Ne laser, and the ruby laser are the most useful because of their relatively high output power and energy and their wavelengths of operation.

The construction of a hologram is basically an exercise in interferometry; therefore good mechanical stability is required during the exposure. If any of the components move enough to shift the fringe pattern at the hologram plane half of a fringe period during the exposure time, then the hologram is ruined. There are two basic techniques for minimizing this problem: isolation of the holographic system from all disturbances, and the use of short exposure times. When a gas laser is used, vibration isolation is generally required, because the power output from the laser is not large enough to permit short exposure times. For the specific system we have constructed using a relatively powerful argon ion laser for crystal growth studies, however, exposure times are about 100 $\mu$sec, which is short enough to relax the isolation requirements. For experiments using light reflected from the object, much longer exposure times are generally required and vibration isolation becomes a prerequisite for successful holography. When $Q$-switched ruby laser systems are used, the pulse length is typically about 20 nsec; for this case no isolation is required.

The proper ratio of the intensities of the object and reference beams at the hologram plane is essential to avoid nonlinear effects in the way exposure is mapped into amplitude transmittance in the emulsion and to obtain adequately bright reconstructed images. The reconstructed image would be brightest if the object and reference beams were nearly equal, since in this case the fringe visibility would be greatest. With nondiffuse objects, however, it would be difficult to remain in the linear portion of the $|T_A|$ versus $E$ curve over the entire hologram area. Failure to remain in the linear portion of the $|T_A|$ versus $E$ curve would result in spurious images which can frequently occur in the region of interest. To avoid this effect, a reference wave from 4 to 10 times more intense than the object wave is generally used.

## HOLOGRAPHIC MICROSCOPY

Several techniques have been developed and others suggested which combine holography with microscopy. The advantages of holographic microscopy over conventional microscopy all depend on the complete recording of the amplitude and phase information of the light transmitted by or reflected from the object. The ability to reconstruct the object wave at a later time allows the use of a standard microscope with short working distance and depth of field in examining a relatively large sample volume. The microscope can move through the reconstructed real image and is not constrained by the walls of the original sample chamber. Although, instead of using holography, a relay lens could be used to form a real image for microscopic viewing,

a high quality lens with a large field of view and numerical aperture would be difficult to obtain. Also, the use of a relay lens would not provide the advantages that holographic recording does in studying rapidly changing phenomena. The depth of field and field of view recorded by a hologram are much greater for the same resolution than can be recorded by other techniques; therefore dynamic events which might normally be missed can be recorded and carefully examined at some later time. In addition, since the complete object wave is recorded, special viewing techniques such as dark-field microscopy, interferometry, and phase microscopy can be employed on the reconstructed images to illustrate optimally any details of special interest [18].

Some of the holographic recording techniques used in microscopy are lensless in that the object is directly recorded by the hologram; others employ a lens so that the hologram records a magnified image. With direct recording, variations in the emulsion and its base and changes in the emulsion during and after processing introduce aberrations which degrade the reconstruction and make resolution of object detail as small as 1 $\mu$m impossible. These aberrations can be reduced with careful processing and the use of a flat glass substrate for the emulsion. If maximum resolution is required, however, it is generally better to employ some initial magnification. This decreases the bandwidth that must be recorded by the hologram and makes the effect of the aberrations on the reconstructed image detail proportionately less. Unfortunately the use of a lens also reduces the sample volume that can be recorded and, except for the technique introduced by Toth and Collins [19] (discussed in a later section), introduces the normal distortion present with any lens; that is, the longitudinal magnification is equal to the square of the transverse magnification. If a larger sample volume is desirable and if only moderate magnifications are required, then a lensless holographic recording technique may be preferred. In the following sections three arrangements will be discussed, two of these employing initial magnification by a lens and one using the direct recording technique.

**Modified Conventional Microscope**

A holographic microscope developed by van Ligten and Osterberg [20] is shown in Fig. 8. In this arrangement the object is magnified by the microscope objective and a hologram is formed with an off-axis reference wave. Image detail to 1 $\mu$m is readily recorded in this manner.

As was previously mentioned, one advantage of this technique over conventional microscopy is the large depth of field recorded. For example, Lawton and van Ligten [21] have shown that the depth over which 1-$\mu$m detail can be resolved in conventional microscopy employing an objective with a numerical aperture of 0.6 is approximately 0.6 $\mu$m. With holographic microscopy this depth is increased to 250 $\mu$m. An off-axis reference wave is used in this technique; therefore a high-resolution emulsion is still required, although the spatial frequencies that must be recorded are not as great as in the other techniques, since a relatively small reference angle can be employed. Only a low-power laser is required, because the field of view recorded is small, as is the area of the hologram. As an example, holograms of transparent specimens have been recorded on Agfa-Gevaert Scientia 14C70 film with a 4-mW He-Ne laser. The exposure times were of the order of 1 msec.

A commercial version of this microscope is now available. If 1-$\mu$m resolution is required and microscopic fields of view are adequate, then this approach to holographic microscopy could be the most satisfactory and economical. To record a larger sample volume, one of the other techniques would be required. The best approach must be determined by the problem of interest.

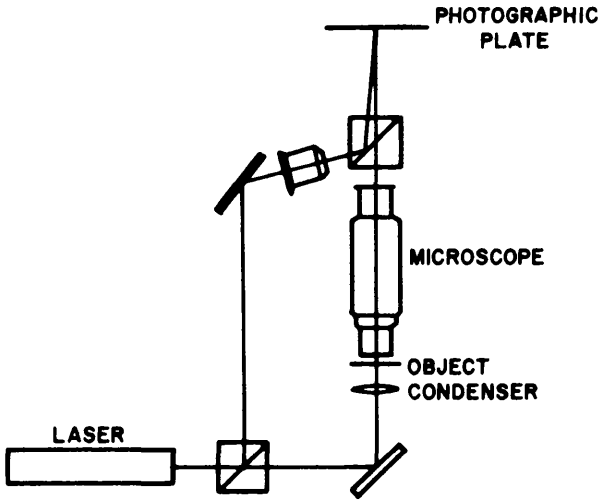


Fig. 8 – A holographic microscope as employed by van Ligten and Osterberg [20]

**Intermediate-Lens Technique**

A technique employing an intermediate lens which reduces the effect of the aberrations introduced in the holographic recording process was described by Toth and Collins [19]. In this arrangement (Fig. 9) a plane wave is incident on the sample volume from the left. The light deflected by the sample is collected by the lens and forms the object wave at the hologram plane. A plane off-axis reference wave is used as shown. The real image is reconstructed from the hologram through the same intermediate lens and then viewed with an ordinary microscope.

One advantage of this technique is that, since a magnified image is recorded, the effects of the aberrations introduced by the holographic emulsion and substrate are reduced. Another advantage is that a relatively inexpensive lens with a large numerical aperture can be used; thus a larger sample volume can be recorded. This advantage obtains because any aberrations introduced by the lens in the recording process are effectively canceled by the lens when it is used to reconstruct the complex conjugate of the real image. To see this, consider again the arrangement of Fig. 9. If the wavefront at the lens is given by $U(x, y)$ and the effect of the lens is represented by $pe^{jk\xi(x,y)}$, where $\xi(x,y)$ includes the imperfections and aberrations of the lens, then the wavefront leaving the lens is $U(x, y)pe^{jk\xi(x,y)}$. If a hologram is recorded and processed and a complex conjugate of the reference wave is used in the reconstruction, then the third term in Eq. 10 at a plane just before the lens is proportional to $U^*(x,y)pe^{-jk\xi(x,y)}$. On tranversing the lens the wavefront is again multiplied by the factor $pe^{+jk\xi(x,y)}$, and the aberrations due to the lens are canceled.

One further advantage of this technique is that it allows the use of an inexpensive lens as a relay element in situations where the phenomenon to be recorded is inaccessible. It also frequently permits a more convenient recording geometry and allows the off-axis reference wave to be brought in at a smaller angle than would be required without the use of the lens.

Figure 10 is a ray-trace diagram showing the use of an intermediate lens in a holographic arrangement to record the events in a crystal-growth chamber. The simple lens shown has a 50-mm diameter and a 50-mm focal length. A hologram 50 mm in diameter is indicated, which might be recorded on 70-mm film. With this specific arrangement, a sample volume of 3 $cm^3$ can be recorded. The use of larger film would permit the recording of a larger sample volume;

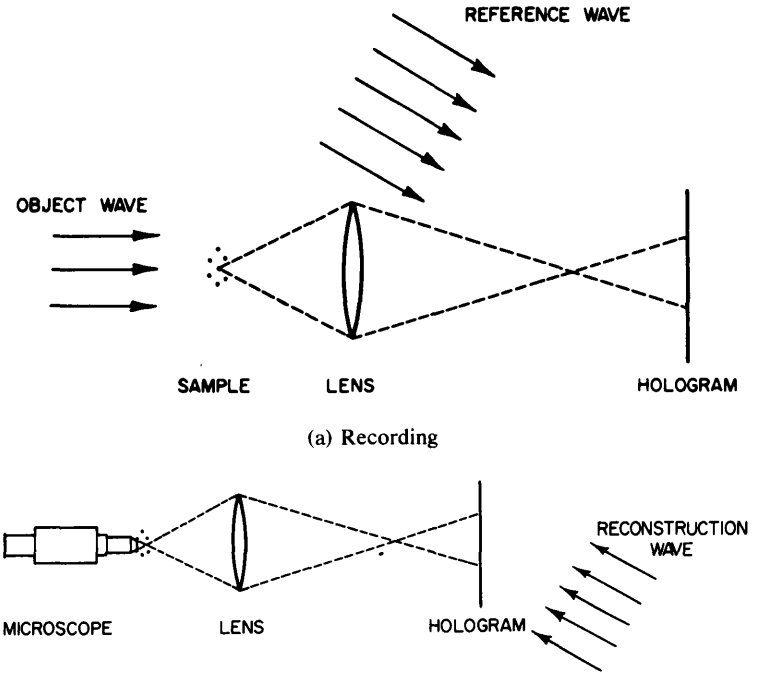


Fig. 9 – Holographic arrangement using the intermediate-lens technique of Toth and Collins [19]

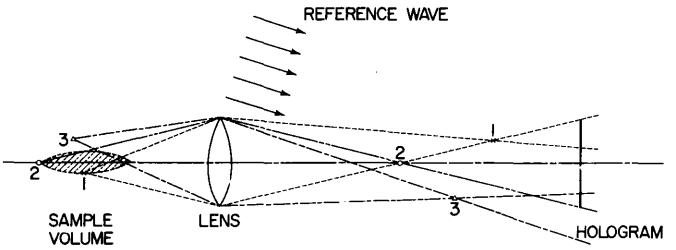


Fig. 10 – The use of an intermediate lens in a holographic arrangement to record events in a crystal-growth chamber. The hologram does not intercept all of the rays forming the image of point 3, so it is not considered to be within the recorded sample volume.

but the resolution is of course determined by the lens. The reference angle and the positions of the sample, lens, and hologram plane are all interrelated. The optimum combination would have to be determined for a specific experiment. To obtain similar resolution with the same size film but without the use of an intermediate lens, the film would have to be placed close to the crystal-growth chamber; this would make the introduction of the off-axis reference wave difficult.

Problems are associated with the accurate placement of the lens in the recording and reconstruction arrangements, but with carefully designed optical mounts these can be overcome. The recording of a test pattern at the beginning of each series of holograms is recommended, as this can be used to adjust the alignment for the entire series.

This technique has been employed by McFee [22,23] for recording sodium nitrate crystal growth in a crucible at 306°C. A thick quartz lens with one end immersed in the crystal melt is used as a relay between the furnace and the hologram plane. Reconstructed holograms show the grain boundaries at the solid/liquid interface, and the resolution of the system has been shown to be about 300 cycles/mm.

High-resolution holographic emulsions are required for this technique because of the relatively large angles used for the off-axis reference waves. Agfa-Gevaert Scientia 8E70 35-mm film was used in the preceding arrangement with a 15-mW He-Ne laser. The exposure times were of the order of 10 msec.

A similar arrangement has been reported by Cox, Buckles, and Whitlow [24]. Their system was used to study the growth of bubbles in the cheek-pouch blood vessels of a hamster confined to a pressure chamber. A pulsed argon ion laser was used, and the holograms were recorded on 16-mm film.

**High-Resolution Direct Holographic Recording**

The remaining technique, that of direct holographic recording, is perhaps the simplest. Its application to crystal-growth studies is shown in Fig. 11. The diffraction-limited resolution of the system is a function of its numerical aperture and is simply determined by the size of the hologram and its distance from the sample. For the geometry shown the object detail with the highest spatial frequency recorded $\nu_m$ is given by

$$\nu_m = \frac{\sin\theta}{\lambda}, \tag{20}$$

where $\lambda$ is the recording wavelength. This is the maximum resolution possible. Factors that can degrade the resolution below this diffraction limit are discussed by Smith [10] and Collier, Burchhardt, and Lin [12].

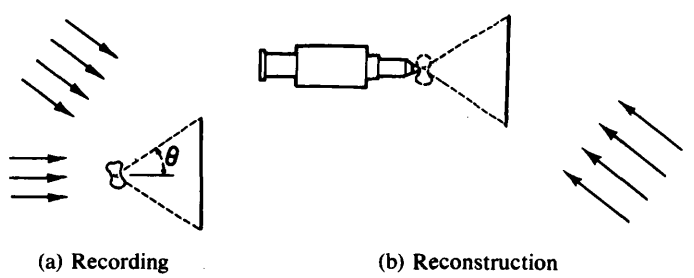


Fig. 11 – Direct holographic recording and reconstruction of specimens with microscopic detail

Whereas this arrangement has the disadvantage of generally providing an image of lower resolution than either the holographic microscope or the intermediate-lens technique, it is the easiest to use in both the recording and reconstruction stages. The resolution can be improved somewhat by increasing the size of the hologram, but special attention must be paid to the hologram itself. If glass plates are used, the emulsion should ideally be on special flat glass so that in the reconstruction step any aberrations through the glass are minimized. When high-resolution film is required to record a series of holograms for some rapidly changing phenomenon, care

must be taken to hold the film flat in both the recording and reconstruction steps. The film would normally be held in a motorized film transport for exposure, and during reconstruction the processed film can be sandwiched between two pieces of flat glass with an index matching oil. The oil serves to remove the effect of the thickness variations of the substrate and emulsion, some of which are caused by the processing. With that technique a test target has been recorded and reconstructed with a resolution of 600 lines/mm.

The requirements on the laser used in this technique are little different from those required when an intermediate lens is used. For our experimental arrangement we have chosen a CW argon ion laser producing 2.5 watts at 514.5 nm in the $TEM_{00}$ mode. Typical exposure times using Agfa-Gevaert Scientia film or plates are about 100 $\mu$sec with a hologram area of 20 $cm^2$ (using a plane reference wave with a diameter of 50 mm). With transparent specimens the coherence length of the source is not of great importance, since the path lengths of the reference and object wave can be readily equalized to within a few centimeters—less than the coherence length of either He-Ne or ion lasers.

The primary advantage of this technique for holographic microscopy, as already stated, is in the relative ease of alignment of the components for reconstruction of the real image. The hologram must be aligned only with respect to the reference beam, but this alignment is extremely critical for maximum resolution. The use of a high-resolution test target is again helpful. A secondary advantage is that the sample volume that can be recorded with this arrangement is larger than with either of the preceding arrangements for a given film size and other system parameters.

## INTERFEROMETRIC TECHNIQUES

Holographic microscopy offers unique opportunities in interferometry. Prior to the development of holography the standard arrangement for viewing phase variations in a transparent specimen was a modification of the Mach-Zender interferometer. In this system the illuminating wavefront is split, one portion passing through the transparent specimen and the other portion passing through a similar optical path but without a specimen. The two wavefronts are then recombined to create interference fringes from local phase variations across the beam which traversed the specimen. Variation of the object beam from a plane wavefront or some other convenient illuminating wave produces these fringes.

There are several forms of holographic interferometry which greatly increase the versatility of microscopic examinations of phase variations [25]. In one form a hologram of some object is made, processed, and carefully replaced in its original position. The lensless hologram recording technique is generally used. The wavefront for the reconstructed virtual image then coincides with the wavefront from the object itself. If the object is now slightly changed in some manner, interference fringes will be observed which indicate the actual change in the object. In this form the comparison wavefront is no longer a plane or spherical wave as in a Mach-Zender or Michelson interferometer but is the complicated wavefront produced by the object itself before the distortion was applied.

A similar comparison is made in double-exposure holographic interferometry. A hologram of the object is made; then a change is introduced and a second exposure on the same emulsion is added to the first. On reconstruction the two images, real or virtual, interfere with each other, forming fringes indicating the change in the object between the two exposures.

The first technique allows the fringes to be viewed in real time as the changes in the object occur and is therefore convenient for studying such phenomena as stress concentration in some structural member as a function of the applied force. However in studies of the continuous process of crystal growth it is desirable to compare the crystal morphologies at two instances in time when there is not a sufficiently long interval between the instances to process and reposition the hologram. Double-exposure holographic interferometry can be applied to this situation. It has the further advantage that it is not susceptible to vibrations during the reconstruction; therefore sharp fringes are easily observed. In studying a continuous process the double-exposure technique permits the average rate of change during an interval of time to be measured. The live fringe technique, on the other hand, allows a continuous measure of the total change.

When a time sequence of single-exposure holograms is recorded, an arrangement employing a Mach-Zender interferometer in either the construction or reconstruction stage can be used to view the total change during some process. This technique is particularly useful in studies of crystal growth, since interference fringes formed between a plane reference wave and the object wave transmitted by the crystal-growth chamber show the deviation of the crystal/liquid interface from a plane. In the arrangement shown in Fig. 12 a plane wave and object wave are recorded simultaneously. On reconstruction frozen fringes are observed. Figure 13 shows the reconstruction of a hologram made with this type of arrangement. The object is a crystal-growth chamber at a time after the start of crystal growth.

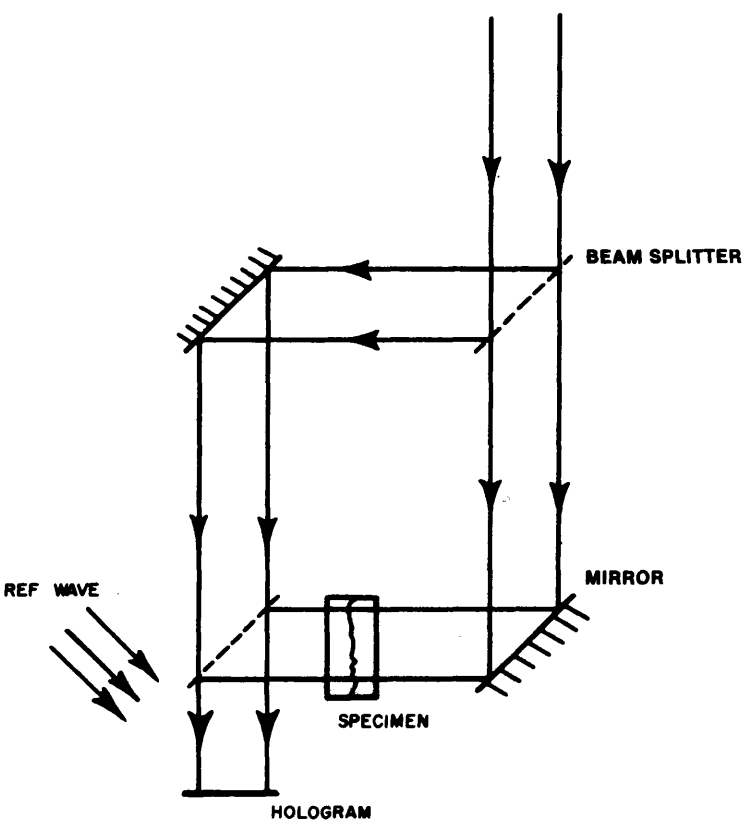


Fig. 12 — Holographic recording of a crystal-growth chamber in a Mach-Zender interfometer

Fig. 13 – Reconstruction of a hologram made with the arrangement shown in Fig. 12

An alternative arrangement shown in Fig. 14 compares the reconstructed real image with a plane wave. This arrangement has the advantage that the spacing and orientation of the interference fringes formed can be adjusted by tilting the plane wave in such a way as to offer the best view of the structure of the features under investigation. The grain boundaries seen in Fig. 15b clearly show surface structure not evident in Fig. 15a. For interference microscopy a further advantage of using the arrangement shown in Fig. 14 is that it is used with a conventional single-exposure hologram which can also be viewed using other standard techniques as previously described. This arrangement does however require vibration isolation to stabilize the interference fringes during reconstruction.

The techniques shown in Figs. 12 and 14 permit a series of holograms to be made and the changes in the crystal surface structure to be studied as a function of time. The interference fringes are all formed by comparison of the object wave with the same plane wave at different stages during the crystal growth.

A modification of the double-exposure technique can accomplish the same objective as a Mach-Zender interferometer. The specimen is simply removed from the object beam for one of the exposures. The hologram, on reconstruction, then exhibits fringes formed by interference between the reconstructed specimen and the undeviated object wave.

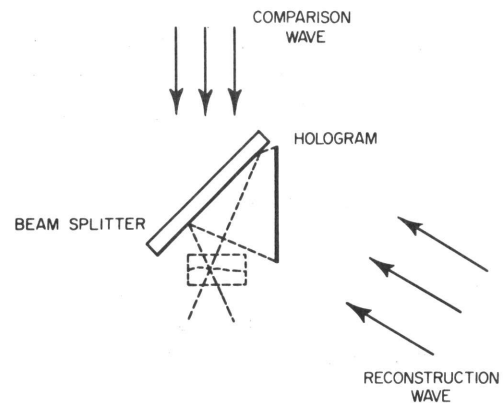


Fig. 14 – Holographic interferometry in which the reconstructed sample image is compared to a simple plane wave

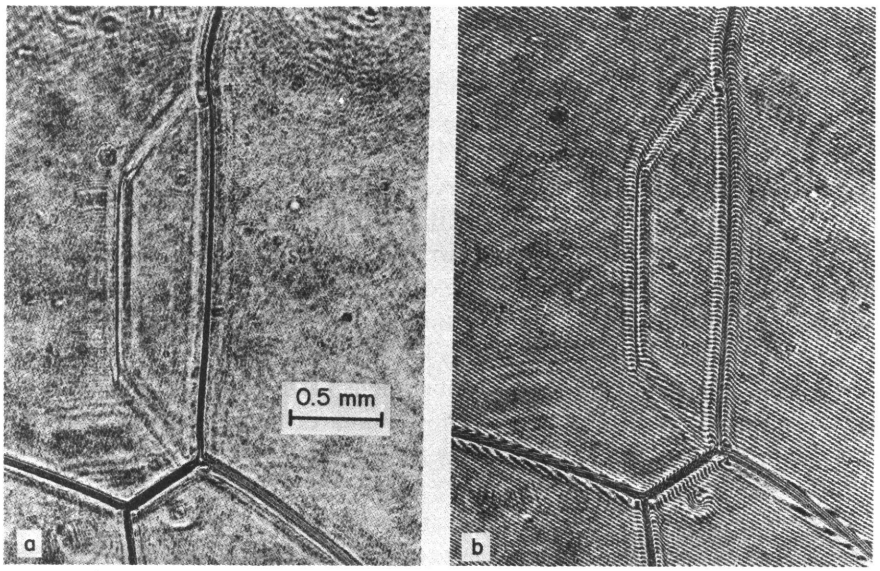


Fig. 15 – Reconstructed image of crystal grain boundaries in camphene (a), and the same image viewed with the arrangement of Fig. 14 (b)

In general the interpretation of the fringes formed for arbitrary object motion is complicated [26,27]. For the arrangement used in crystal-growth studies, however, the motion is primarily parallel to the direction of illumination and of viewing. For this case the fringe spacing corresponds to contours with a separation given by

$$\Delta h = \lambda/\Delta n, \tag{21}$$

where $\Delta n$ is the change in the index of refraction of the crystal material on melting.

A somewhat different form of holographic interferometry has been used by McFee [23], in the work mentioned earlier, to record and measure crystal growth from the melt. This method is applicable to birefringent materials and was applied specifically to sodium nitrate. Interference fringes representing contour lines of constant optical thickness were formed due to coherent addition of the ordinary and extraordinary rays as they were transmitted through the crystal. The fringe interval is a function of the angle between the optical axis of the crystal and the incident beam and varies from $4\lambda$ for the incident beam perpendicular to the optical axis to infinity

for the incident beam aligned along the optic axis. This technique has the advantage that contour fringes are readily produced with no additional optics. The orientation of the crystal must be determined however to calibrate the fringe interval spacing.

## EXPERIMENTAL SYSTEMS

The preceding sections have described some general holographic principles and some specific holographic techniques. This section describes the experimental methods and equipment we have used in a working holography laboratory. Our laboratory has been planned for adaptation to a wide variety of metallurgical research applications. The first application was a study of crystal growth in transparent materials which serve as analogs to solidifying metals. This section will include a discussion of the factors which influence the selection of components in the holography system, including operating convenience.

Crystal growth can be observed conveniently in thin layers of material sandwiched between glass microscope slides, but crystals grown under such circumstances may differ significantly from crystals growing in bulk liquid. To avoid the constraining influence of the container walls on diffusion, convection, and crystal geometry, we used crystal-growth chambers with considerable depth. Because important crystallization events occurred at unpredictable locations within the chamber volume, it was necessary to record the entire volume of the chamber with high resolution. For this purpose, the limited field of view recorded by the modified conventional microscope was not acceptable, so we used the intermediate-lens and direct-recording techniques, although the resulting image resolution is not as high. In practice we preferred the direct-recording technique because of the relative ease of alignment for reconstruction. With this technique we could study crystals growing throughout the volume of test chambers up to 25 mm across and 1 to 25 mm deep with resolution of about 3 $\mu$m.

Figure 16a shows the usual arrangement of the system for high-resolution direct holographic recording. In Fig. 16b, some of the same components are being used to form the reconstructed image. The entire system is rigidly mounted on a vibration-isolation table. Figure 17 is a photograph of our apparatus with all components in place. To obtain the optimum quality in the reconstructed images, each of the components must be carefully selected.

### Laser

The most important component of a holography system is the laser. The light provided by this instrument must be monochromatic and coherent, and the resonant mode of the laser cavity should be $TEM_{00}$. To expose holograms with the desired area in the short exposure times needed for rapidly growing crystals, relatively high laser powers may be required. At slow crystal growth rates the laser power requirements are considerably reduced. When selecting a laser, one should bear in mind that losses in the optical system can often leave only 25% to 50% of the laser power available at the film plane for actually exposing the hologram when using light transmitted through transparent specimens. Still less light is available at the film plane when using light reflected from opaque specimens.

Crystal-growth studies do not generally require the extremely short exposure times attainable with $Q$-switched solid-state lasers. An argon ion laser can provide adequate power for most crystal-growth studies, and in many cases a He-Ne laser can be used. We have found

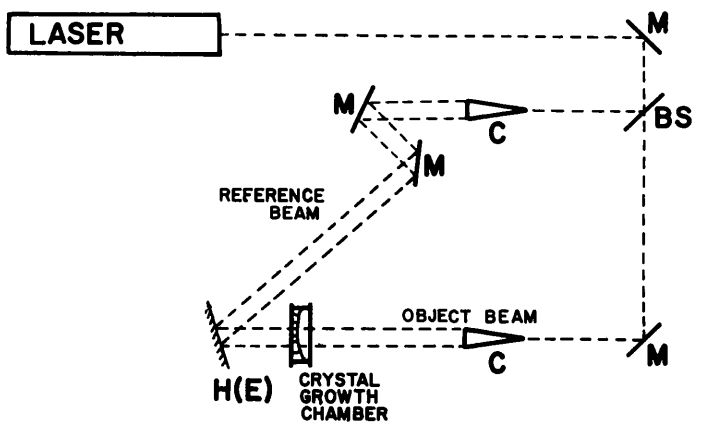


(a) Recording

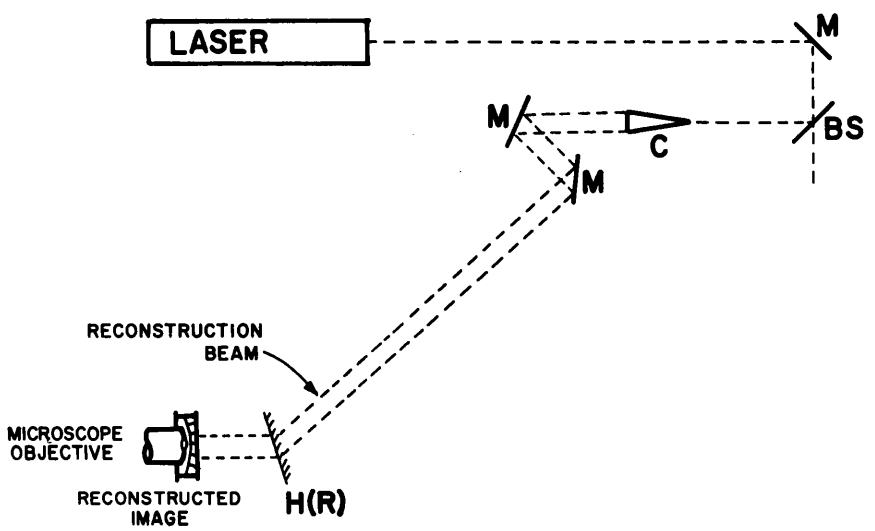


(b) Reconstruction

Fig. 16 — Schematic representation of an optical system for recording and reconstructing holograms. The same collimated beam is used as the reference beam during recording and as the reconstruction beam. The hologram is rotated 180° about a vertical axis for reconstruction, to produce a real image for microscopic examination.

a useful and versatile arrangement to be an argon ion laser with an intracavity $Q$-spoiler (acousto-optical) which allows easy electronic control of exposure time. A prism wavelength selector can be used to eliminate all but one line of the argon spectrum. Argon ion lasers generally produce about equal intensity at 488.0 and 514.5 nm, but the latter is preferred because of the eye's greater sensitivity at this wavelength. The laser we used in these experiments generated 2-1/2 watts at 514.5 nm, and the resulting exposure times were generally 50 to 500 $\mu$sec.

## Table

When short exposure times are possible ($\lesssim$100 $\mu$sec), excellent holograms can be made without the need for vibration isolation equipment. If longer exposure times are required, or

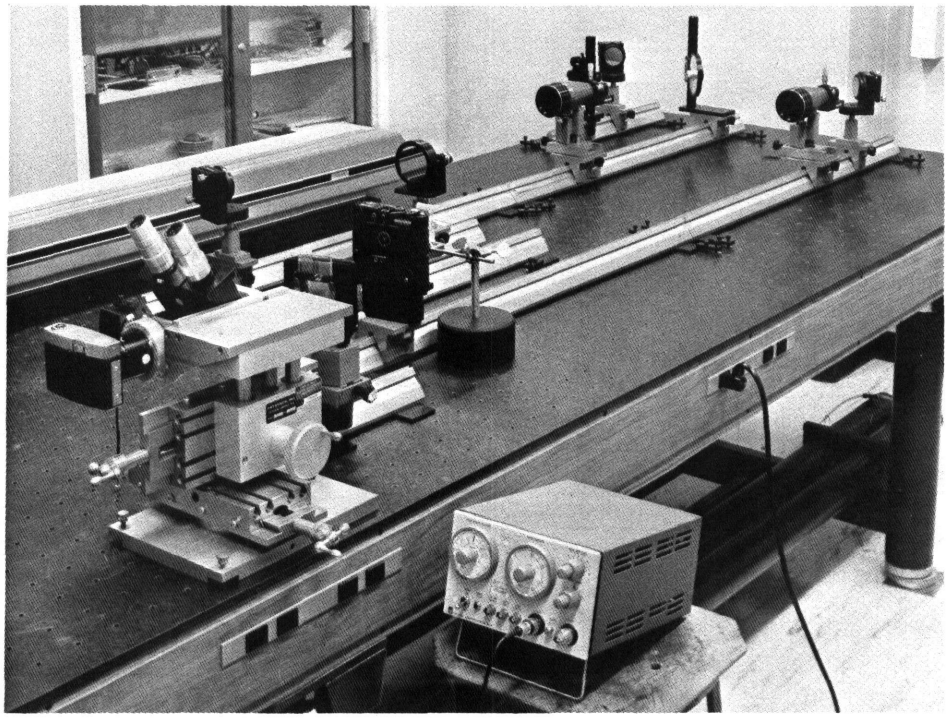

Fig. 17 — Holographic system, as used in crystal growth studies, on a vibration-isolation table. The crystal-growth chamber in this view is almost hidden by the camera body, which holds the holographic film.

if interferometric techniques are used in the reconstruction stage, it is often necessary to mount the holography apparatus on a vibration-isolation table. Considerations of weight and economy tend to favor lightweight honeycomb table tops (as used in our experiments) over massive granite table tops, but the lightweight tops can suffer from acoustical pickup from air conditioners, power supplies, etc.

**Optical Components**

The coherence properties which make laser light so useful for optical interference applications place extra demands on the optical quality of the components in the holography system. Unwanted reflections, or light scattered from dust particles, can create conspicuous interference patterns which seriously degrade the desired image. Moreover any aberrations in the image can produce confusing fringes which are more troublesome to the observer than the diffuse fuzziness produced with incoherent light. Light which has been scattered by dust particles can be eliminated by lens-pinhole spatial filters, which conveniently form a part of the beam-expanding collimators. By placing the filter-collimators as late as possible in the optical paths, most of the dust-scattered light is eliminated. Some of the aberrations are reduced by the use of mirrors and beam splitters with good flatness ($\lambda/10$ or better). The effects of aberrations in any lenses in the system can by minimized by careful alignment of the lens with the optical axis. The intermediate-lens technique of Toth and Collins described earlier removes the aberrations introduced during exposure by canceling them during reconstruction.

The higher cost of dielectric, as opposed to metallic, mirrors often is justified, because the dielectric mirrors can have reflectivities of over 99% for specific wavelengths and angles, as

opposed to a maximum of about 90% for metallic mirrors. When several successive reflections are required, the power losses in metallic mirrors can rapidly become large enough to demand the use of a higher power laser. In such a case the total cost of the system would probably be increased.

**Film**

Many materials are presently in use as media for recording holograms, and more are currently being developed. Most of these media are intended for special applications, such as erasable memories for computers. In the recording of holograms for permanent retention, the sensitivity and convenience of conventional silver halide emulsions are difficult to match. Therefore this discussion is limited to these materials.

Several manufacturers produce films and plates with resolution adequate for holographic applications. Sensitivity decreases rapidly with increasing resolution and is frequently significantly wavelength dependent. Properties of some of the more commonly used materials are listed in Table 1. In the system described here we used Agfa-Gevaert Scientia 10E56 plates and 35-mm films. Although developing procedures for these plates and films do not differ greatly from those for more conventional materials, carefully controlled temperature, time, and agitation are needed if reproducible results are expected.

For most of the crystal-growth applications considered here we made no use of the special properties of thick or volume holograms. Films or plates with thin emulsions could therefore be used.

Table 1 – Holographic Recording Materials

| Material | Holographic Resolution* (cycles/mm) | Exposure $\lvert T_A \rvert = 0.5$ (ergs/cm$^2$) | Approximate Wavelength for Exposure (nm) |
|---|---|---|---|
| Photographic Emulsions | | | |
| Eastman Kodak 649F | >3000 | 800 | 400 to 700 |
| Agfa-Gevaert Scientia | | | |
| 10E56 | 2800 | 10 | 400 to 550 |
| 10E75 | 2800 | 20 | 600 to 700 |
| 8E56 | 3000 | 100 | 400 to 550 |
| 8E75 | 3000 | 75 | 600 to 700 |
| Dichromated gelation | >3000 | $10^5$ | 500 |
| Photoresist | >1000 | $10^5$ | 500 |
| Photopolymer materials | >1500 | $10^4$ | 300 to 700 |
| Photochromic materials | >3000 | $10^6$ | 300 to 500 |
| Electrooptic crystals ($LiNbO_3$) | 4000 | $10^6$ | 500 |

*Resolution is limited by the wavelength of the light used in recording.

Because severe aberrations can be introduced by emulsion shrinkage or warping, the best holograms are usually obtained with emulsions on glass plates. Several plate holders are commercially available with which the exposed plate can be removed for processing and replaced precisely in its original position for reconstruction. This eliminates the need for tedious realignment to obtain the optimum reconstruction. It also makes possible real-time holography, in which the reconstructed image is precisely superimposed on the specimen itself and the two are compared interferometrically. As an alternative to the replaceable plate system, one can use an in situ processing system in which the plate is placed within a glass chamber and the hologram is developed by chemicals circulating through the chamber, without moving the plate at all.

When several holograms are to be made in rapid succession, the use of glass plates is inconvenient. Roll film mounted in a motorized camera body can be used, but the camera body must have a geometry which allows object and reference beams to impinge on the film plane at an adequate angle and with sufficient area of overlap. Most single-lens-reflex camera bodies are relatively thick because of the mirror used, and this restricts the size and angle of the reference beam. A motorized rangefinder camera with a focal-plane shutter has been found to be useful because of its much thinner construction.

**Sample-Growth Chambers**

Many of the holographic techniques described in this report work most effectively in studies of transparent crystals, in which the object beam can pass directly through the specimen, and the hologram records the transmitted light. Glass-walled crystallization chambers can readily be devised with provisions for temperature control appropriate to the particular crystallization phenomenon under study. Figures 18, 19, and 20 illustrate three types of cells which have been useful as crystallization chambers. These cells are constructed from microscope slides and glass tubing, joined together by epoxy cement.

The cell in Fig. 18 is designed to maintain a nearly flat, stable solid/liquid interface by establishing a temperature gradient in the specimen chamber. In this two-chambered cell the upper chamber is wrapped with several turns of resistance wire energized by a power supply with controllable current. The upper chamber is filled with any convenient transparent liquid, which serves as a medium to transfer heat to the lower chamber. The lower chamber is filled with

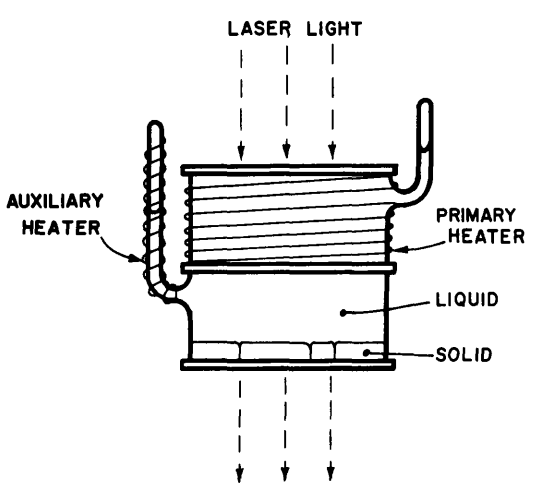


Fig. 18 – Two-chambered cell for study of planar solid/liquid interfaces. The upper chamber contains a transparent liquid for heat transfer, and the lower chamber is filled with the test substance.

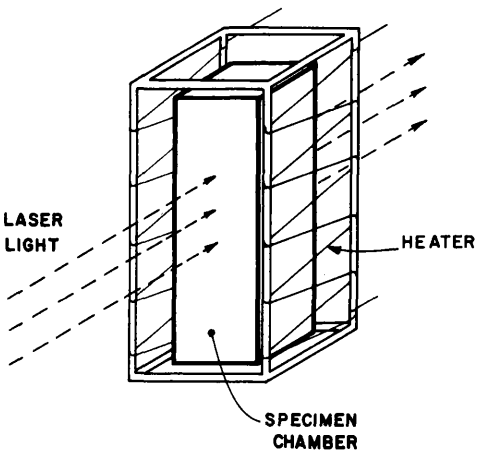


Fig. 19 – Crystallization cell, 25 mm by 25 mm by 75 mm, for observing crystals growing in bulk liquid

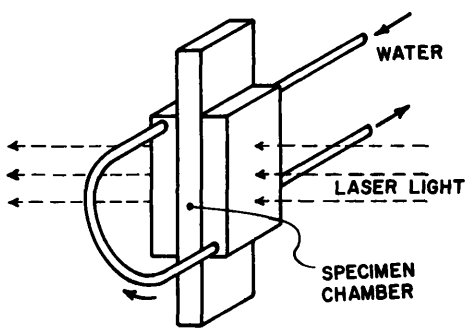


Fig. 20 – Cell for study of crystallization with temperature controlled by circulating water

the substance under study, which has a melting point above room temperature. When power is applied to the resistance heater, the material in the upper part of the lower chamber is melted, and a horizontal solid/liquid interface is established. If the heater power is held constant for 15 to 30 minutes, the interface anneals to a smooth flat surface, except for slight perturbations near imperfections in the crystalline solid. Crystal growth or melting at this initially planar interface can be studied by changing the heater power. The influence of thermal convection in this cell is minimized by introducing the heat from directly above the solid/liquid interface.

A side arm on the lower chamber is equipped with an auxiliary heating coil, which is energized before the main heating coil. In this way the crystal is melted first in the side arm, where space is available for expansion. When the liquid zone extends down the side arm into the main body of the lower chamber, the main heating coil can be energized without danger of breakage.

The cell illustrated in Fig. 19 is designed for observation of cystals growing within bulk liquid. Heating wires are wrapped around an external frame. This type of cell is useful for studies of two-component mixtures, which freeze over a range of temperatures and can produce large numbers of freely floating crystals.

When careful control of specimen temperature is needed, cells such as that in Fig. 20 can be used. The material under study is contained in a central chamber approximately 1 mm thick. On both sides of the central chamber are external chambers through which water circulates with controllable temperature. The temperature of the circulating water is recorded with a thermocouple. This type of cell is useful for experiments in which the specimen is to be studied at carefully controlled constant temperatures, or where carefully controlled temperature changes are desired.

**Reconstruction Techniques**

The ultimate quality of the reconstructed image depends as much on the reconstruction process as on the exposure process. It is easy to underestimate the true quality of a hologram when the observed quality may in fact be limited by the reconstruction process. In studies of crystal growth important features may have characteristic dimensions of only a few microns. These features can be resolved only by a microscope with a large numerical aperture, and such microscopes normally have short working distances. We make our holograms therefore with a collimated reference beam and observe the reconstructed real image as illustrated in Fig. 16b.

Because it may not be possible to replace the hologram during reconstruction in the same mounting device which it occupied during exposure (when roll film was held in a camera body, for example), it is important to have available some method for accurately aligning the hologram with the reconstruction beam. A hologram of a high-resolution test target can be mounted in a tilting device with micrometer adjustments, which are then set to obtain maximum resolution in the reconstructed image. The other holograms in the series can then be substituted for the test hologram without changing the tilt adjustments.

The major operational difficulty of using roll film, as opposed to glass plates, appears to be in maintaining the flatness of the film. If the film is held in simple (and convenient) cardboard mounts for reconstruction, it is often conspicuously nonplanar, and the reconstructed image may be aberrated badly. Good film flatness can be attained by sandwiching the film between two pieces of flat glass (such as 1/8-inch-thick plate glass), with a refractive-index-matching liquid (n-butyl phthalate) between the glass and the film. This procedure results in a substantial increase in image quality, at the expense of considerable extra labor in mounting the holograms.

Flatness during reconstruction is useful only if the film was flat during exposure. Inspection of the film in our camera body revealed that the camera's pressure plate was only partially successful in producing film flatness, and the slight waviness of the film (near the sprocket holes) may have been a limiting factor in image quality.

**Photomicrography**

Photomicrographs of the reconstructed image are most readily recorded on 35-mm or Polaroid film. For detailed examination throughout the reconstructed image, our microscope was mounted on an XYZ translation device (Fig. 17). Because of the low diffraction efficiency of the holograms and the high magnifications with which the reconstructions were observed, long exposure times, up to 5 seconds in some cases, were required. When interference techniques are used, vibration can cause difficulty by introducing jitter in the fringes, which may thus be washed out in the recorded image. The use of fast film, processed for increased sensitivity, helps by reducing the required exposure time.

The microscope camera shutter itself can introduce vibrations which ruin an image which appears stable to the eye. To avoid these one can use an external shutter (not mounted on the vibration-isolation table). A device such as an intracavity accousto-optical shutter, if available, is completely vibration free but can cause difficulty with thermal drift of the laser's resonant cavity when its duty cycle is switched from one appropriate to viewing to one appropriate to photography.

## APPLICATIONS TO CRYSTAL-GROWTH STUDIES

The primary objective of the crystal-growth studies described here is a better understanding of the solidification of metals. Examination of the microstructure of metallic solids frequently reveals that the growth of the component crystals must have been a highly complex process. Because the opacity of metals severely limits the possibilities for experimental study of crystal forms during growth, we have used transparent substances as analogs to metals in solidification studies. Jackson and Hunt [28] have demonstrated that certain organic materials with low entropies of fusion have important similarities to metals in their solidification behavior. In particular these materials solidify from the melt with unfaceted solid liquid interfaces, as do metals. Although these materials differ significantly from metals in some properties, such as thermal conductivity, which are important in solidification, they appear to simulate closely many of the crystal morphologies which occur in metals. For persons not primarily interested in metals, many other crystal morphologies, including faceted growth forms, could be studied holographically with great benefit.

The specific substances we chose for these studies were camphene, succinonitrile, and cyclohexanol, the last being used only as an "alloying" addition to the first two. Both camphene and succinonitrile have body-centered-cubic crystal structure, as do many common metals, and both have convenient melting points just a few degrees above room temperature. We purified these materials before use by repeated zone-refining, but there was indication that some impurities were reintroduced when the materials were transferred to the observation cells.

For interferometric study of these substances we measured the refractive indices in both solid and liquid state with a refractometer. For succinonitrile $n_s = 1.4320$ and $n_\ell = 1.4172$ ($\Delta n = 0.0148$), and for camphene $n_s = 1.4838$ and $n_\ell = 1.4560$ ($\Delta n = 0.0278$). The resulting fringe spacings, delineating differences in crystal thickness, are given by Eq. 21 as 35 $\mu$m/fringe in succinonitrile and 18.5 $\mu$m/fringe in camphene.

### Planar Interfaces

Metallic single crystals with high perfection and homogeneity can be grown from the melt if a smooth planar solid/liquid interface can be maintained. Therefore considerable study has been devoted to determining the factors which influence the stability of planar interfaces [29-34]. Holographic interferometry is well suited to studies of instabilities developing on initially planar interfaces, and we used the cell illustrated in Fig. 18 for this purpose. We obtained planar interfaces by establishing a steady-state temperature distribution in the cell and maintaining this for 15 to 30 minutes. The solid, in a thin layer at the bottom of the lower chamber, usually consisted of several crystals or subcrystals. Through a microscope the grain boundaries were barely visible.

When we reduced power to the heating coil, the solid started to advance into the liquid, and growth features began to develop on the interface. Holograms were recorded as the interface changed from a flat and almost featureless surface to a crowded array of unstable growth forms. We made a few double-exposure holograms in which the first exposure was of the equilibrated flat interface and the second was of the interface after an interval of growth. Unfortunately it is possible to record only one double-exposure hologram for each growth experiment, thus precluding a study of the evolution of a given feature. More frequently we used the Mach-Zender interferometer technique in either taking or reconstructing the holograms, or we made double exposures in which one exposure was a simple plane wave. By making a series of holograms during a single growth cycle, we studied the development of individual growth features.

Figure 21 is a reconstruction from a double-exposure hologram in which the first exposure recorded the equilibrium interface and the second exposure was taken after 60 seconds of growth. The fringes reveal that growth was most rapid near the outside of the chamber, as expected from considerations of the macroscopic heat flow. Because of this inhomogeneous growth rate, regions near the edges of the cell frequently exhibited more rapid morphological development than that of regions near the center.

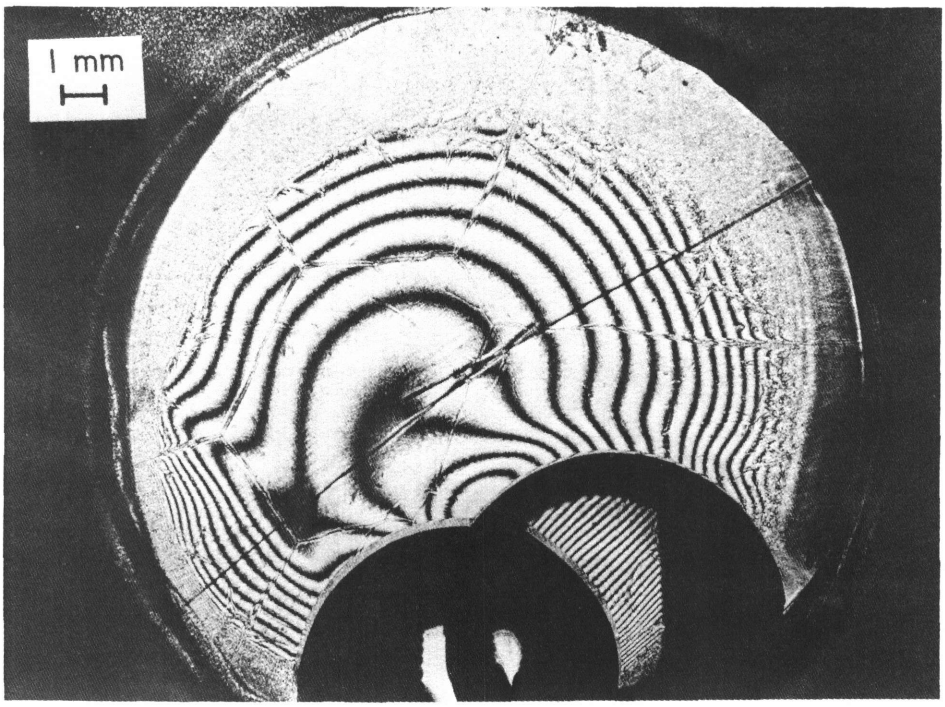


Fig. 21 – Reconstruction from a double-exposure hologram of succinonitrile crystals growing in the cell of Fig. 18. The fringes indicate contours of constant crystal-growth distance with a contour interval of 35 $\mu$m. Two bubbles have affected the growth rate locally. A small thermocouple crosses the cell diagonally.

Microscopic study of reconstructed holograms revealed the prominent role of crystal imperfections in the initiation of surface features. Soon after growth started, grain boundaries and subboundaries became conspicuous as a result of their distortion of the surrounding interface. Interference fringes revealed (Fig. 22) that the interface groove at the boundary, which is shallow at equilibrium, deepened rapidly during growth. The crystal adjacent to the groove grew more rapidly than the general interface, forming a pair of parallel ridges on either side of the groove. The ridges grew until their amplitude was approximately equal to their width and then broke down into rows of regularly spaced individual hills. Individual hills of larger amplitude usually appeared adjacent to crystal trijunctions; these larger hills and some of the regular hills along the ridges later developed into dendrites.

Relative boundary energies could be estimated by observing the dihedral angles at boundary trijunctions, and we found that even boundaries with low energies produced the parallel ridge structure. One boundary in Fig. 23 has insufficient energy to produce any significant deflection of a high-angle boundary, yet it has generated conspicuous surface relief.

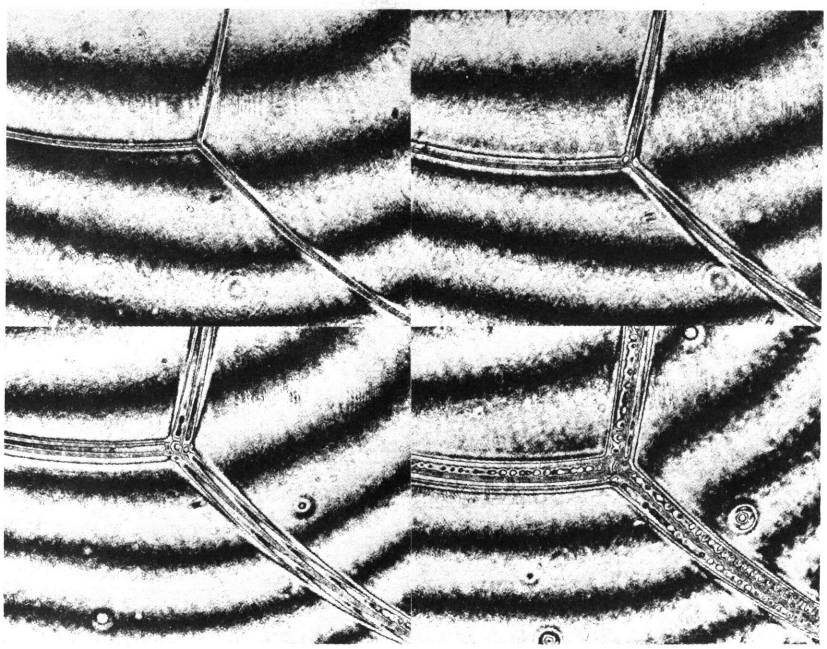

Fig. 22 – Development of features near a crystal trijunction at a solid/liquid interface. These camphene crystals are reconstructed from holograms recorded by the Mach-Zender interferometer technique of Fig. 12. Ridges growing adjacent to the grain boundaries in the top left, top right, and bottom left break into rows of individual hills in the bottom right.

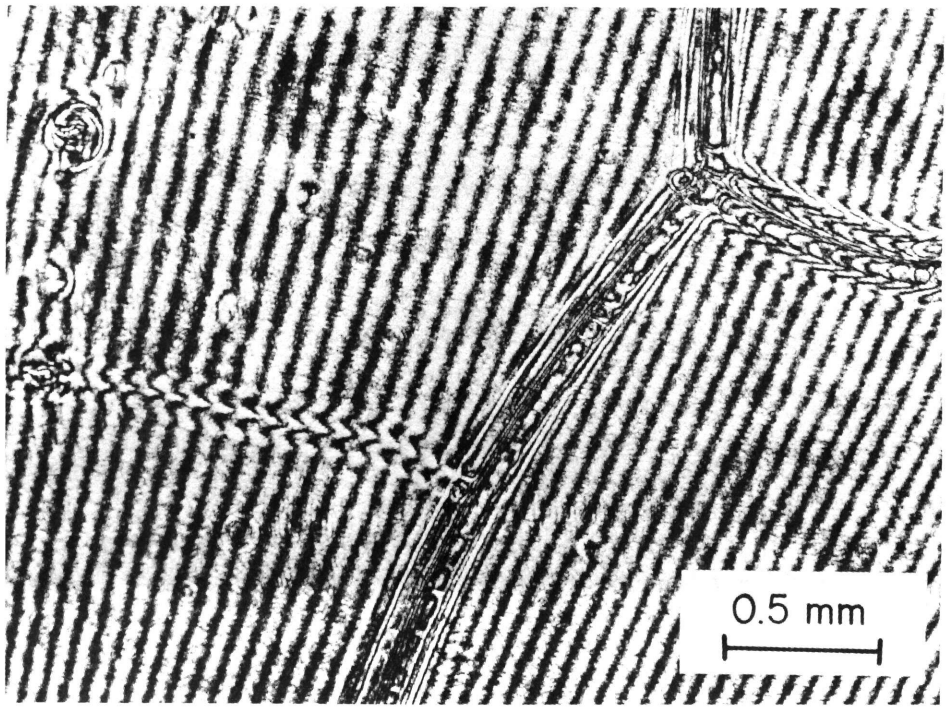


Fig. 23 – Distortion of a solid/liquid interface in camphene by a low-energy crystal subboundary (left). A Mach-Zender interferometer was used in the reconstruction (Fig. 14).

A similar phenomenon is observed where undissolved impurity particles are engulfed by the advancing solid. Such particles cause pits in the surface, which then become surrounded by annular ridges. One such pit with its surrounding ridge is seen in Fig. 24.

The behavior of the interface near grain boundaries can be ascribed to the influence of impurities rejected by the solid as it starts to advance into the liquid. These impurities will accumulate in the liquid ahead of the interface and thus retard the growth of the solid everywhere except near the grain boundaries, where the impurities can move laterally into the grain-boundary groove. The groove will thus deepen, and the regions adjacent to it, having the groove available as a sink for impurities, will grow more rapidly. This is the same mechanism proposed by Morris and Winegard [35] to explain segregation patterns near grain boundaries in a dilute Pb-Sb alloy.

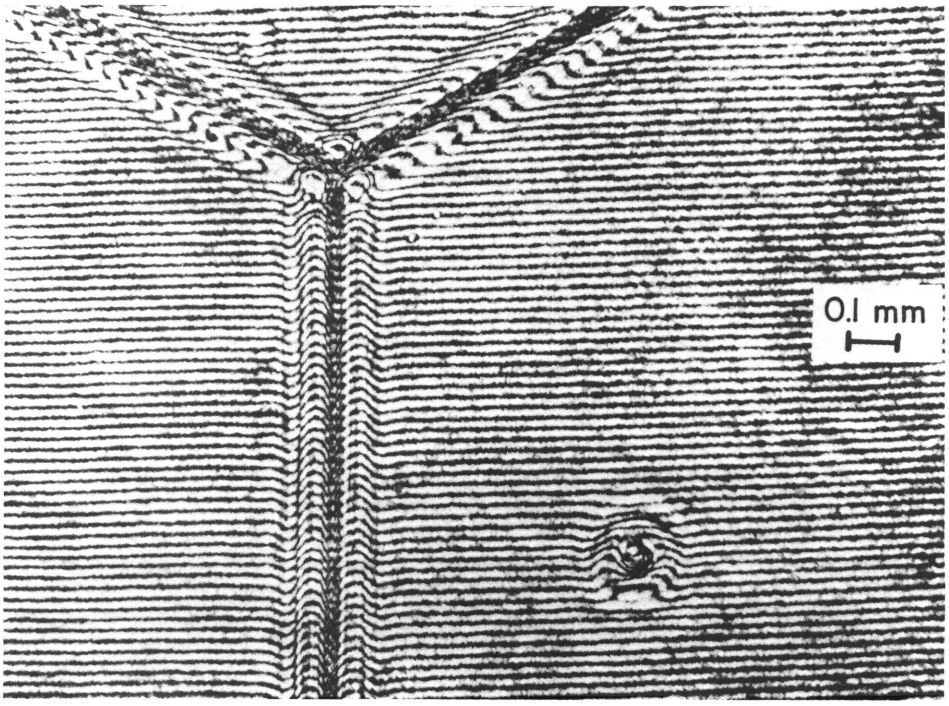


Fig. 24 – Circular ridge surrounding a pit in a camphene crystal.
The pit is caused by an impurity particle.

Several theoretical treatments of planar interfaces merely address the question of whether the planar interface is stable [29-31,33,34], whereas other treatments attempt to calculate the period and growth rate of features which are unstable [32]. The growth conditions assumed in these treatments (constant growth velocity and an initially planar interface) cannot be obtained readily in experiments. In practice one can study time-dependent growth forms on unstable planar interfaces only by starting with stationary interfaces and observing growth at an accelerating rate. Thus a numerical comparison between these experiments and the theoretical analyses is difficult, although a meaningful qualitative comparison is possible.

The dynamic treatments of planar-interface stability normally assume as a starting shape a planar interface with an infinitessimal periodic perturbation. Individual interface features of small amplitude can be represented as a sum of periodic functions. The time-dependent analysis

by Sekerka [32] predicts the development of an interface feature initially resembling a grain-boundary groove. The predicted interface shapes are similar to those observed experimentally (Fig. 25) until the amplitude of the features becomes comparable to their wavelength. The two-dimensional geometry then breaks down into the row-of-hills structure, and the wave propagation suggested by the theory in later stages does not occur.

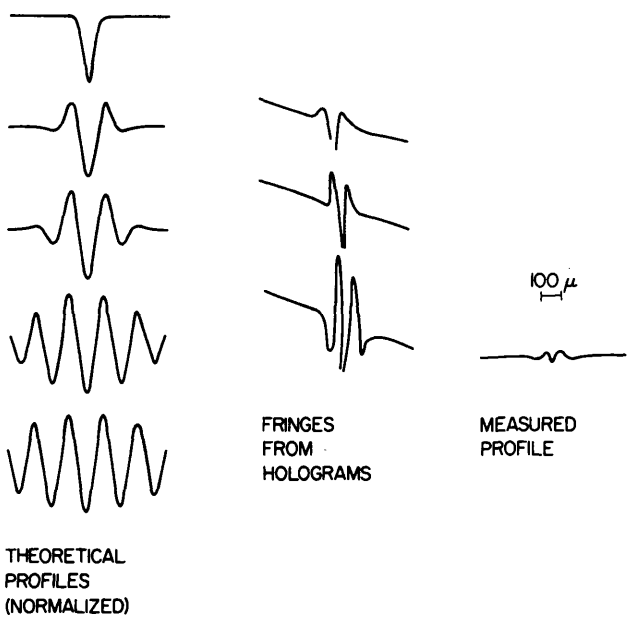


Fig. 25 – Interface shapes as predicted by time-dependent theory [32] and as measured from interference fringes near grain boundaries

The fringe patterns reveal that secondary grooves are usually formed outside of the primary ridges, and in infrequent cases weak secondary ridges are formed outside of these secondary grooves (Figs. 22 and 23). However there was never any indication of long-range periodic structures propagating outward from grain boundaries.

Regions not adjacent to grain boundaries or impurity particles remained smooth even when the features near the imperfections had attained considerable amplitudes. Eventually however a general roughness developed over the entire crystal surface (Fig. 26). Features with a random rather than periodic distribution soon covered the entire crystal surface.

**Dendrites**

Crystals growing rapidly under conditions in which heat or solute or both diffuse away from the crystal into the liquid frequently assume a dendritic form. The growth and branching of dendrites is an important part of the microstructural development of metals. Because of the great difficulty of mathematically analyzing branching growth, theoretical treatments frequently have been confined to studies of the extreme tip of the dendrite. Even the analysis of this relatively simple shape is difficult when the effects of surface energy and crystallization kinetics are included.

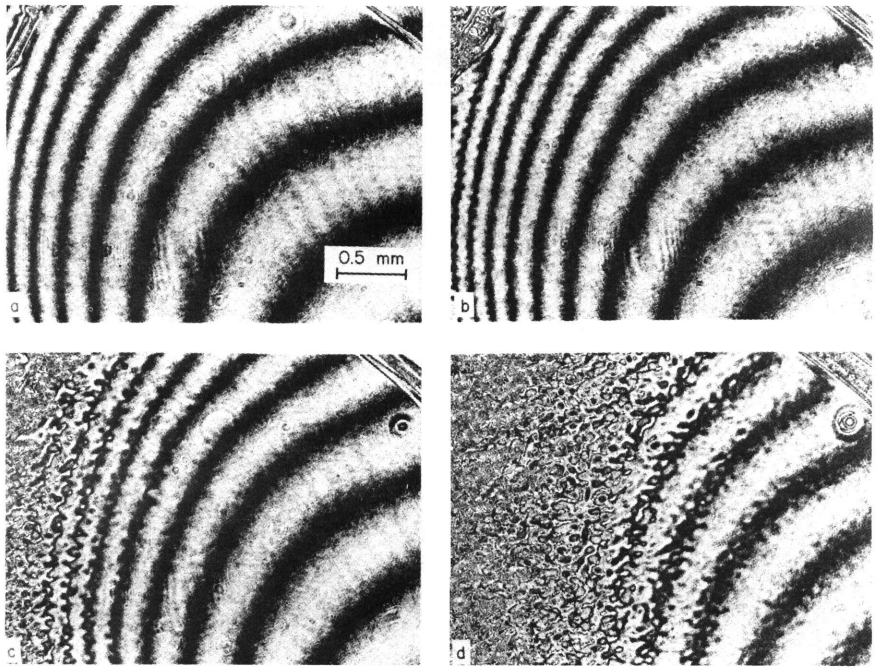


Fig. 26 — Development of general roughening on an initially smooth solid/liquid interface, from the same holograms used in Fig. 22.

Most theories have treated the dendrite tip as a paraboloid of revolution, even though this cannot be exactly correct [36]. Tin dendrites growing on the surface of molten tin were shown to resemble parabolas near their tips [37], but few other attempts to measure tip shapes have been reported. Holographic interferometry can be used to measure the shape of dendrites of transparent materials in the region near the tip and in some cases quite far back into the branched region.

We occasionally encountered dendrites during our studies of planar interfaces in the cell of Fig. 18. When we allowed the cell to cool rapidly by turning off the power to the heating coils, dendrites sometimes grew across the field of view from the side walls of the lower chamber. Although most of these were rapidly obscured by growth features developing on the crystalline layer at the bottom of the cell, the tips of the dendrites remained visible in some cases and could then be studied. We used interference microscopy to measure the cross-sectional shape of these dendrite tips. In Fig. 27 the fringes traced from a succinonitrile dendrite are compared with those calculated under the assumption that the tip is a body of revolution. Because the exact shape of the experimental fringes is difficult to follow where they bend sharply at the edge of the dendrite, the difference between the theoretical and experimental fringes is not considered to be significant.

The cell shown in Fig. 20 was also used for studies of dendritic growth. Hot water was first circulated through the two outer jackets to melt the material in the central part of the observation chamber. The water temperature was then gradually decreased, and dendrites grew across the field of view from the unmelted ends of the observation chamber. Because these dendrites were confined to a region only 1 mm thick, many of them could not grow or branch in the preferred crystallographic directions. This restriction had a conspicuous influence on the mode

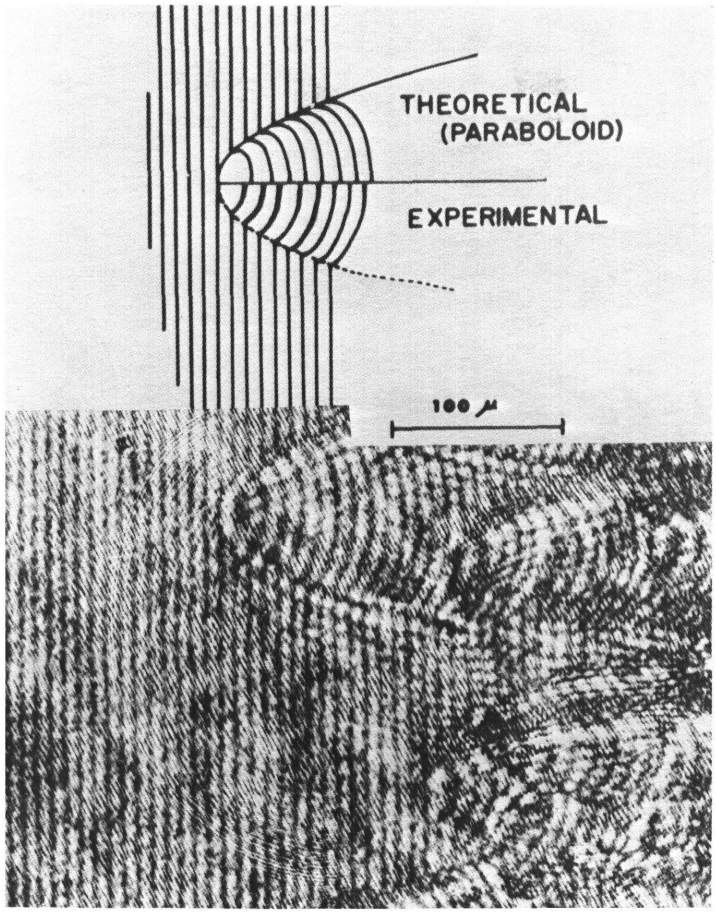


Fig. 27 – Comparison of fringes calculated for a perfect paraboloid of revolution with fringes traced from a dendrite tip in succinonitrile

of propagation of the dendrites. Although dendrites with favorable orientations grew with orthogonal branches and steady-state paraboloidal tips, the behavior of nearby dendrites with less favorable orientations was significantly different (Fig. 28). They frequently showed tips which did not resemble paraboloids and did not propagate in a steady-state manner. Instead the tips grew and divided in a periodic manner. This process often resulted in a dendrite with an extremely regular branch spacing, but the branches were not orthogonal to the main stem.

When dendrites developed into fully three-dimensional structures with secondary and tertiary branches, interferometry was no longer possible. Only the initial stages of branching, and branches confined to essentially two-dimensional regions, were well suited to study by holographic interferometry. Branches in their initial stages of growth (near the tip) and branches confined to small amplitude by the chamber walls or by neighboring dendrites usually had highly regular spacing. As the branches grew, some of them were eliminated by competition from their neighbors, so the spacing of the surviving branches was somewhat irregular and greater than the original spacing (Fig. 29). The original, regular spacing should be predicted by theories of dendrite tip stability, whereas the final spacing of surviving branches also depends on competition and ripening effects.

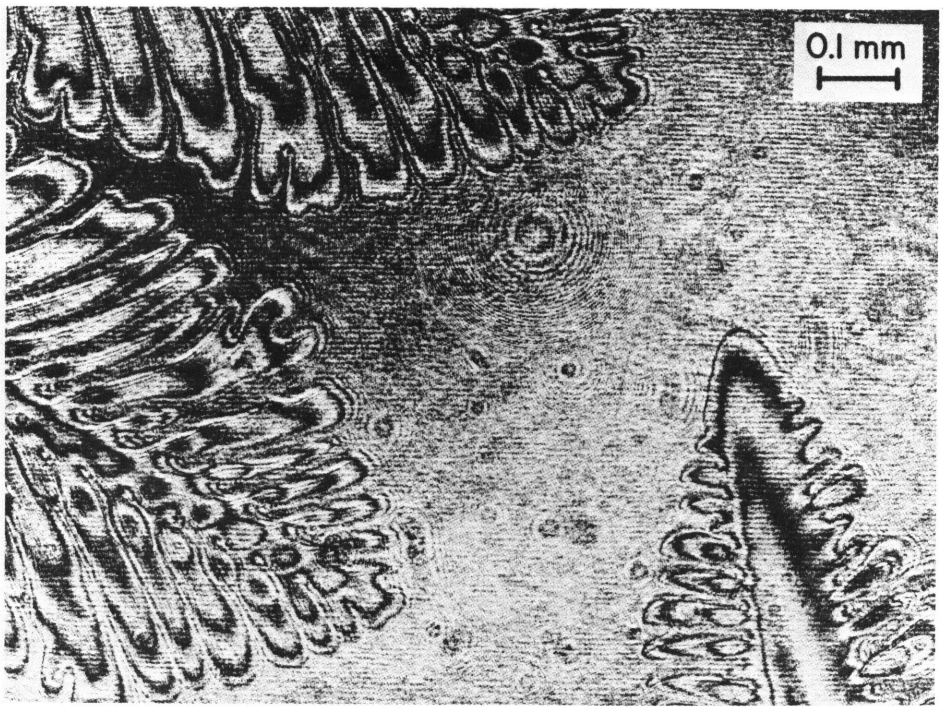


Fig. 28 — A camphene dendrite growing in the preferred gowth direction, with a paraboloidal tip, and dendrites growing in unfavored directions, with periodically dividing tips

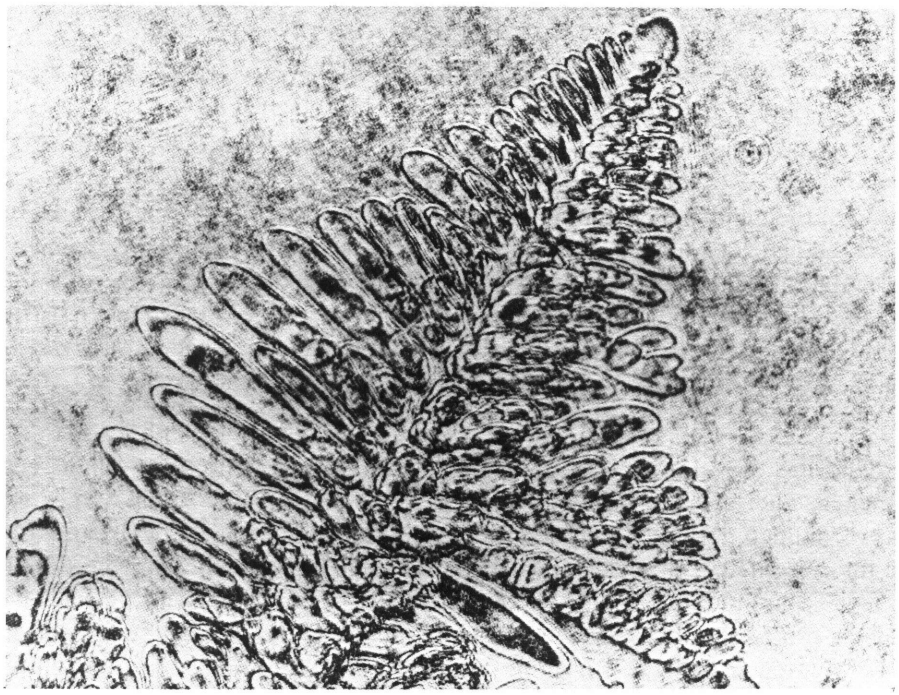

Fig. 29 — Dendrite with regular spacing near the tip and less regular spacing farther back where some branches have been eliminated by competition

Although the observations of dendritic growth indicate that crystal anisotropy plays an important role, they do not reveal whether this role is played by the surface energy, the interface kinetics, or some other property. The growth of the dendrite is too complex to permit a simple relation between the dendrite behavior and the detailed behavior of the contributing processes. To clarify the role of the individual processes, it is fruitful to study simpler geometries.

**Freely Floating Crystals**

The growth of an isolated, initially spherical crystal presents an easier situation for analysis than does the growth of a dendrite. Observations can be studied in terms of the deviation from the spherical shape. If the sphere is fairly small compared to the diffusion distance characteristic of the crystal growth process, the effects of anisotropy become conspicuous. Fortunately such small crystallites can be produced quite easily in a two-component system by the fragmentation of dendrites.

We prepared a mixture of camphene and 11% cyclohexanol and sealed it within the cell shown in Fig. 19. At room temperature this mixture equilibrates as a two-phase system, with camphene-rich solid and cyclohexanol-rich liquid. When heated a few degrees above room temperature, the system becomes totally liquid; dendritic freezing takes place upon subsequent cooling to room temperature. During dendritic freezing a few small floating crystals of uncertain origin usually appear in the center of the cell. These correspond to the equiaxed crystals frequently found in a metal ingot. The number of these crystals can be increased vastly by briefly reheating the cell during the dendritic growth stage (Fig. 30). A multitude of dendrite fragments is then formed and swept to the center of the chamber by convection currents, and many of these fragments melt back to spherical or cigarlike shapes before growth starts again.

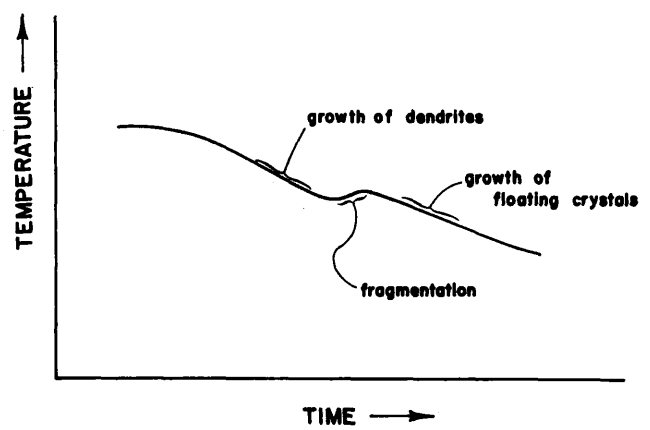


Fig. 30 — Cooling cycle to produce dendrite fragments for study of floating crystals

We recorded holograms as these small crystals grew into dendritic equiaxed crystals. We obtained adequate resolution only when we used glass plates to record the holograms, which we usually recorded as double exposures, with 5 to 10 seconds between exposures. During this interval the crystals drifted far enough so that two spatially separated images were recorded. Each of these images was combined with an image of the unobstructed object beam (from the

other exposure), so each image showed thickness fringes generated as in the plane-wave double-exposure technique. The change in crystal size during the interval between exposures was generally too small to provide the basis for a useful measurement.

Because the hologram reconstructs in sharp focus hundreds of crystals throughout the volume of the test chamber, it was not difficult to locate crystals having a symmetry axis reasonably well aligned with the optical axis of the viewing microscope. The interference fringes were then easily interpreted to reveal the exact shape of the crystal, especially when the optical axis was aligned with a ⟨100⟩ direction in the crystal.

As soon as crystal growth started, the influence of crystallographic anisotropy became apparent (Fig. 31). Crystals changed from the almost spherical shape developed during melting to rounded octahedra, as growth proceeded most rapidly in ⟨100⟩ directions. Growth proceeded at the corners of the octahedra at an accelerating rate, with each of the six corners developing into an approximately paraboloidal dendrite tip. The first stages of branching appeared soon after the octahedral stage passed.

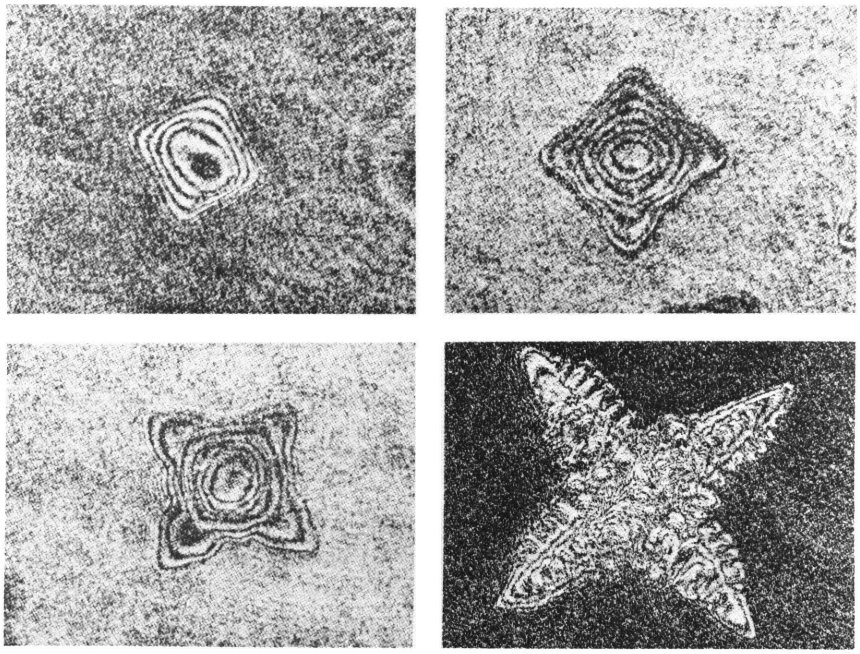

Fig. 31 – Small crystals developing from an octahedral shape to dendritic equiaxed form in a mixture of camphene and 11% cyclohexanol. The symmetry of the growth forms indicates the important role of crystal anistropy.

Cigar-shaped fragments were also present, these being protions of dendrites which had originally grown in ⟨100⟩ directions, so that the axis of the fragments lay along a ⟨100⟩ direction. These elongated fragments grew by developing an octahedral knob at each end, with a dendrite developing from each corner of the knob (Fig. 32). Periodic ripples also developed along the axis of the fragments, but these did not generally grow into dendrites.

The symmetry of the growth forms developing from both spherical and elongated fragments indicates that convection does not play a significant role at this stage in the development of

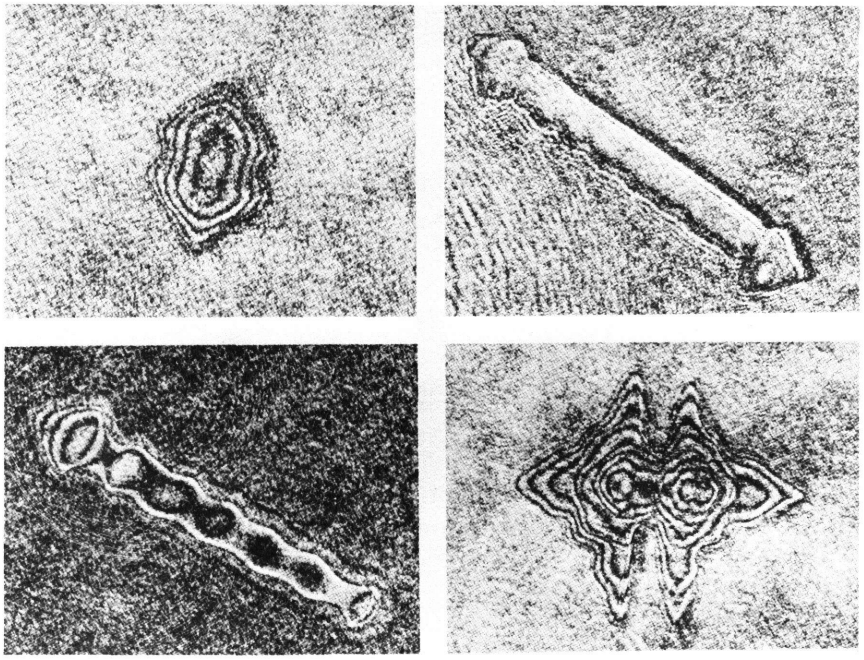

Fig. 32 — Four examples of the development of initially cigar-shaped crystals in a mixture of camphene and 11% cyclohexanol

the crystal morphologies, because convection could not have an equal effect at all six corners of an octahedron. Instead there appears to be relatively little motion between a crystallite and its diffusion field.

**Liquid Inclusions**

Although the free-floating crystals reveal the important influence of crystal anisotropy on the initial development of dendritic crystals, they do not reveal whether the anisotropy is due to the influence of surface energy or to that of interface reaction kinetics. Anisotropy of the solid/liquid interface energy could be measured by measuring the equilibrium shape of the floating crystals, but their transient existence makes this impractical. Not only do they rapidly sink to the bottom of the container, but they undergo large variations in size when subjected to only small fluctuations in temperature. Fortunately the equilibrium shape can be determined quite easily by the study of the similar situation in which liquid inclusions occur within single crystals.

Consider a two-component system with a simple phase diagram such as that shown in Fig. 33. At temperature $T_0$ the equilibrium state of systems with compositions anywhere between $\alpha$ and $\beta$ will consist of solid of composition $\alpha$ and liquid of composition $\beta$. At system composition $B$, close to $\beta$, we could have small crystals of composition $\alpha$ in a large volume of liquid of composition $\beta$, whereas at system composition $A$, close to $\alpha$, we could have small inclusions of liquid of composition $\beta$ within large crystals of composition $\alpha$. The compositions of solid and liquid in equilibrium at the interfaces are identical for system compositions $A$ and $B$. Thus the interfacial energies and equilibrium shapes should be the same in the two cases. The liquid inclusions are much easier to study, however, because they remain fixed in place within the crystal and because they are relatively stable when subjected to slight changes in temperature.

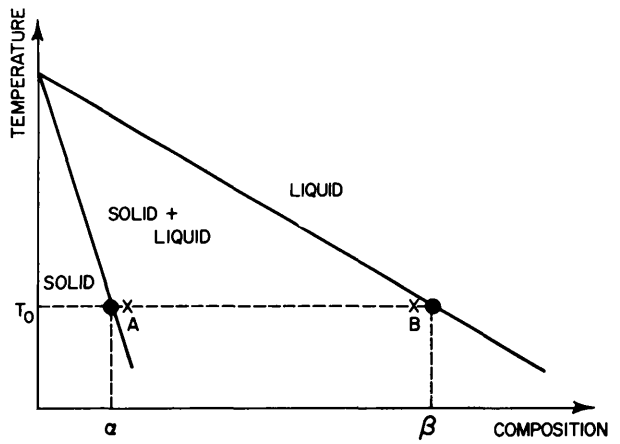


Fig. 33 – Phase diagram of a simple binary system, illustrating the equivalence of overall composition B (small crystals of composition $\alpha$ in a liquid of composition $\beta$) and overall composition A (liquid inclusions of composition $\beta$ in a solid of composition $\alpha$).

For the studies of liquid inclusions we filled the cell of Fig. 20 with a mixture of camphene and 2% cyclohexanol. We allowed this material to freeze dendritically, with solute-rich interdendritic material remaining liquid at room temperature. After several days this interdendritic liquid had collected into small isolated droplets within the bulk of the camphene crystals. We measured the equilibrium shape of these droplets to determine the anisotropy of the solid/liquid surface energy (Fig. 34) and found the anisotropy in the camphene-cyclohexanol system to be approximately 2%.

When we cooled the system, the liquid inclusions shrank by inward growth of the surrounding crystal. If the cooling rate was large enough, the crystal grew into the inclusion in a dendritic mode. The orientation of the crystal could be determined by observing the ⟨100⟩ growth directions of the dendrites within the inclusions (Fig. 35). By this means we found the orientation with the maximum surface energy (Fig. 34) to be ⟨100⟩.

Lower cooling rates, insufficient to produce dendritic growth, produced shrinkage of the liquid inclusions with more moderate shape changes. The small anisotropy of the inclusions evident at equilibrium was greatly accentuated when the inclusions were shrinking. When we heated the system, the inclusions grew larger and the shape anisotropy diminished until the inclusions became almost spherical. This behavior can be compared to that of the freely floating crystals, which become rounded on heating (diminishing size) and become more anisotropic on cooling (increasing size).

Crystal-growth theories for unfaceted systems have generally concluded that at small supercooling the interfacial kinetic process is relatively unimportant as a rate-limiting step [38,39]. This conclusion is supported by our observations of crystallites and inclusions reported here. If the anisotropy of crystal growth rates were controlled by anisotropic interface kinetics, the crystal growth rate would be fastest in the same crystallographic direction for both growth of crystallites and shrinkage of inclusions. Instead, we find that those directions (⟨100⟩) which show the fastest rates during growth of the crystallites are the directions which show the slowest rates during the shrinkage of the inclusions.

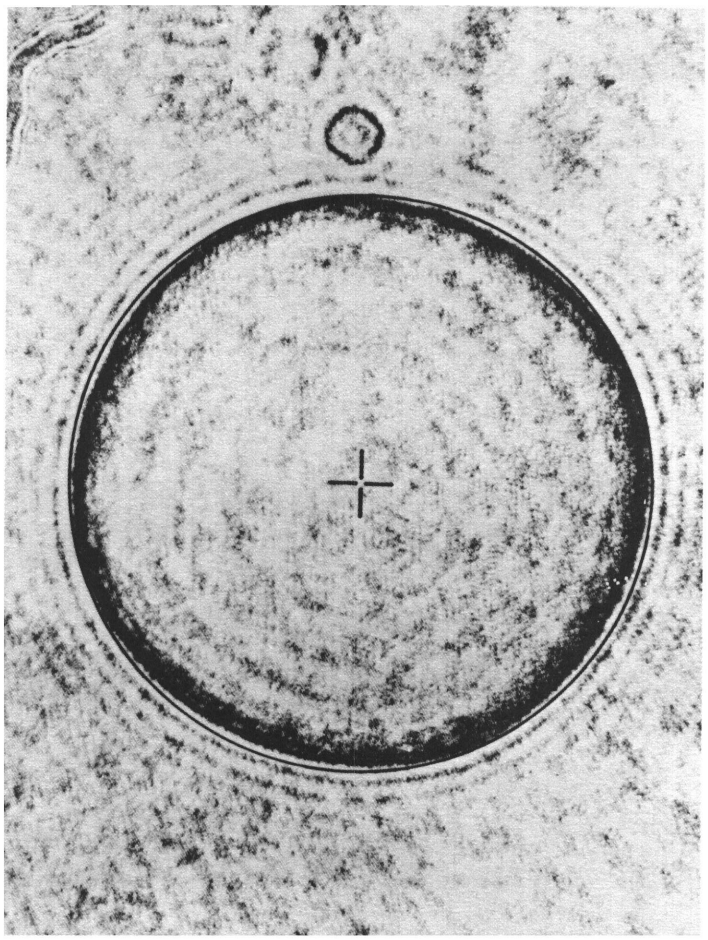

Fig. 34 — Equilibrium shape of a cyclohexanol-rich inclusion in a camphene crystal. A circle has been circumscribed to illustrate the small anisotropy, approximately 2%.

If the effects of interface kinetics are assumed to be negligible, the shape changes can be readily understood in terms of the redistribution of solute in the liquid phase as an initially anisotropic body changes size. Figure 36 illustrates schematically the growth and shrinkage of crystallites and inclusions, showing in each case the expected distribution of solute and shape change. The anisotropy of the figures has been exaggerated for clarity. The diffusion of solute in the liquid phase is influenced by the initially anisotropic shape, and the local growth rates are functions of the local solute concentrations. We conclude that one does not have to call upon any significant effect from interface kinetics to explain the growth and shrinkage of crystallites and inclusions in unfaceted materials.

A strikingly different behavior is seen in systems in which the solid/liquid interface is faceted. In these systems the interfacial kinetic process can play an important rate-limiting role at small supercoolings. Interfaces tend to become faceted when there is no easy way for new crystal layers to start to grow or dissolve, but the interfaces become rounded when these layers can start at corners. Consequently crystals surrounded by liquid become rounded as they melt

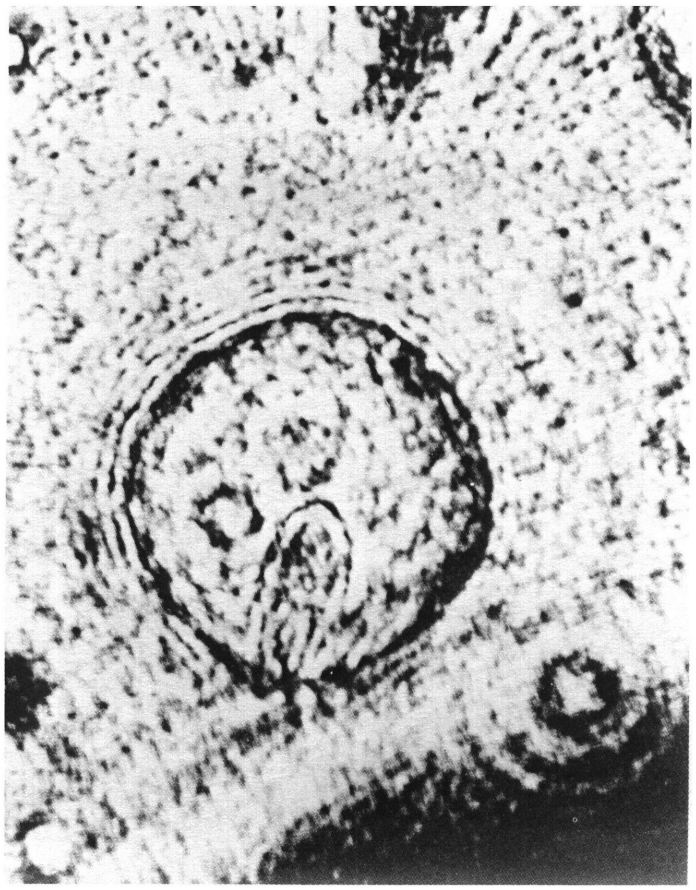

Fig. 35 — Rapidly cooled inclusion, with a dendrite indicating the ⟨100⟩ direction

and faceted as they freeze, but inclusions within crystals become faceted as they expand (melting) and rounded as they contract (freezing). Such behavior has been observed in bismuth single crystals melted in the electron microscope [40] and in freezing and melting films of salol [41].

**Summary**

Holography offers unique advantages in crystal-growth studies over conventional microscopic techniques. The images of crystals growing throughout the volume of a relatively large experimental test chamber can be recorded with high resolution. Since both the amplitude and phase of the object wave are recorded, interferometric techniques can be used to measure precisely the shape and growth rate of the crystals. Holography thus makes possible some severe tests of theories of crystal-shape stability.

The experimental system described here will record several off-axis holograms per second with individual exposure times of approximately 100 $\mu$sec. The reconstructed images permit detailed study of sample volumes of a few cubic centimeters with a resolution as high as 400 cycles/mm.

In deciding whether to use holographic or conventional microscopic techniques for a given application, one must weigh holography's inherent advantages against its disadvantages of

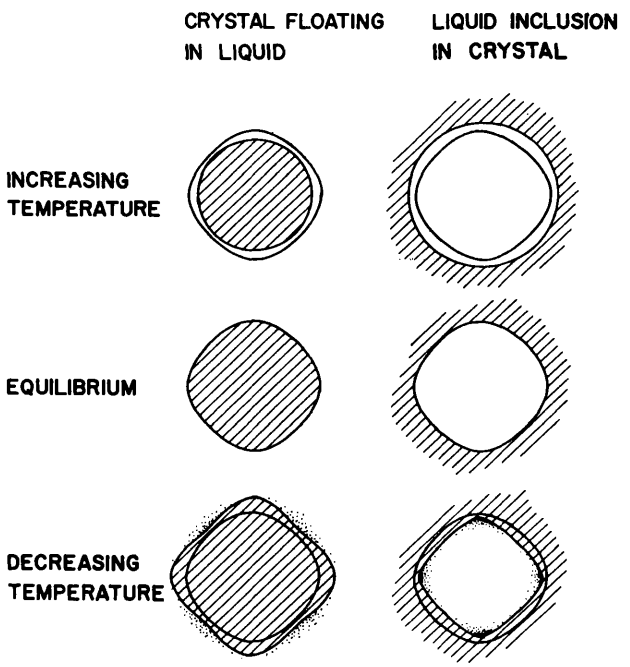


Fig. 36 – Shape changes of floating crystals and liquid inclusions within crystals, with changes of temperature. The equilibrium shape is shown for comparison in each case. The local solute concentration, retarding the growth of the crystal, is indicated by dots for the case of decreasing temperature.

increased complexity, somewhat lower resolution than conventional microscopy, and increased image noise due to the use of coherent illumination. In the applications described here the use of holographic techniques is justified.

Holographic studies of transparent organic analogs to solidifying metals have revealed that crystal imperfections such as grain boundaries, subboundaries, and foreign particles can initiate surface relief features on solid/liquid interfaces but that these features do not propagate as waves for long distances across the interface.

The tips of dendrites which are free to grow in their preferred crystallographic direction were found to be close to steady-state paraboloids. Dendrites constrained to grow in other directions show different tip shapes, frequently changing with time in a more or less periodic manner.

The influence of crystal anisotropy was studied in freely floating crystals and in liquid inclusions within crystals by observing the shape changes resulting from temperature changes. The observed growth forms can be explained on the basis of diffusion and anisotropy of the surface energy, with interfacial kinetic effects apparently playing an unimportant role at small growth rates.

## REFERENCES

1. D. Gabor, Nature **161** (1948) 777.
2. D. Gabor, Proc. Roy. Soc. (London) **A197** (1949) 454.

3. D. Gabor, Proc. Phys. Soc. (London) **B64** (1951) 449.
4. E.N. Leith and J. Upatnieks, J. Opt. Soc. Amer. **52** (1962) 1123.
5. E.N. Leith and J. Upatnieks, J. Opt. Soc. Amer. **53** (1963) 1377.
6. E.N. Leith and J. Upatnieks, J. Opt. Soc. Amer. **54** (1964) 1295.
7. G.W. Stroke, *An Introduction to Coherent Optics and Holography,* 2nd edition New York, Academic Press, 1969.
8. J.B. DeVelis and G.O. Reynolds, *Theory and Applications of Holography,* Reading, Massachusetts, Addison-Wesley, 1967.
9. J.W. Goodman, *Introduction to Fourier Optics,* New York, McGraw-Hill, 1968.
10. H.M. Smith, *Principles of Holography,* New York, Wiley-Interscience, 1969.
11. H.J. Caulfield and S. Lu, *The Applications of Holography,* New York, Wiley-Interscience, 1970.
12. R.J. Collier, C.B. Burckhardt, and L.H. Lin, *Optical Holography,* New York, Academic Press, 1971.
13. E.N. Leith, J. Upatnieks, and K.A. Haines, J. Opt. Soc. Amer. **55** (1965) 981.
14. R.W. Meier, J. Opt. Soc. Amer. **55** (1965) 987.
15. H. Kogelnik, in Proc. Symp. Modern Opt., J. Fox, editor, Brooklyn, Polytechnic Press, 1967.
16. C.B. Burckhardt and E.T. Doherty, Appl. Opt. **8** (1969) 2479.
17. K.S. Pennington and J.S. Harper, Appl. Opt. **9** (1970) 1643.
18. R.F. van Ligten, in *Holography,* S.P.I.E. Seminar Proceedings **15,** 1968.
19. L. Toth and S.A. Collins, Jr., Appl. Phys. Letters **13** (1968) 7.
20. R.F. van Ligten and H. Osterberg, Nature **211** (1966) 282.
21. K.C. Lawton and R.F. van Ligten, in *Developments in Holography,* S.P.I.E. Seminar Proceedings **25,** 1971.
22. R.H. McFee, J. Appl. Phys. **40** (1969) 3873.
23. R.H. McFee, Appl. Opt. **9** (1970) 1834.
24. M.E. Cox, R.G. Buckles, and D. Whitlow, Appl. Opt. **10** (1971) 128.
25. A.E. Ennos, pp. 199-260 in *Advances in Quantum Electronics,* Vol. 1, D.W. Goodwin, editor, New York, Academic Press, 1970.
26. K.A. Haines and B.P. Hildebrand, Appl. Opt. **5** (1966) 595.
27. B.P. Hildebrand, *A General Analysis of Contour Holography,* Univ. of Michigan, Willow Run Laboratories, Institute of Science Technology, Report 7421-35-T, Feb. 1968; available from Defense Documentation Center as report AD 828931.
28. K.A. Jackson and J.D. Hunt, Acta Met. **13** (1965) 1212.
29. J.W. Rutter and B. Chalmers, Can. J. Phys. **31** (1953) 15.
30. W.A. Tiller, K.A. Jackson, J.W. Rutter, and B. Chalmers, Acta Met. **1** (1953) 428.
31. W.W. Mullins and R.F. Sekerka, J. Appl. Phys. **35** (1964) 444.
32. R.F. Sekerka, J. Phys. Chem. Solids **28** (1967) 983.
33. R.T. Delves, Phys. Stat. Sol. **16** (1966) 621.
34. R.T. Delves, Phys. Stat. Sol. **17** (1966) 119.
35. L.R. Morris and W.C. Winegard, J. Crystal Growth **5** (1969) 361.
36. G.F. Bolling and W.A. Tiller, J. Appl. Phys. **32** (1961) 2587.
37. M.E. Glicksman and R.J. Schaefer, Acta Met. **14** (1966) 1126.
38. M.E. Glicksman and R.J. Schaefer, J. Crystal Growth **1** (1967) 297.
39. R.J. Schaefer and M.E. Glicksman, J. Crystal Growth **5** (1969) 44.
40. M.E. Glicksman and C.L. Vold, Acta Met. **15** (1967) 1409.
41. D.P. Woodruff, Phil. Mag. **18** (1968) 123.

Security Classification

## DOCUMENT CONTROL DATA - R & D

*(Security classification of title, body of abstract and indexing annotation must be entered when the overall report is classified)*

| | |
|---|---|
| 1. ORIGINATING ACTIVITY *(Corporate author)*<br>Naval Research Laboratory<br>Washington, D.C. 20390 | 2a. REPORT SECURITY CLASSIFICATION<br>UNCLASSIFIED<br>2b. GROUP |

3. REPORT TITLE

"DESIGN AND APPLICATIONS OF A HOLOGRAPHIC SYSTEM FOR CRYSTAL GROWTH STUDIES"

4. DESCRIPTIVE NOTES *(Type of report and inclusive dates)*
Summary report on a continuing problem.

5. AUTHOR(S) *(First name, middle initial, last name)*
J. A. Blodgett and R. J. Schaefer

| | | |
|---|---|---|
| 6. REPORT DATE<br>January 2, 1973 | 7a. TOTAL NO. OF PAGES<br>45 | 7b. NO. OF REFS<br>41 |
| 8a. CONTRACT OR GRANT NO.<br>NRL Problems N01-16.101 and M01-23.101<br>b. PROJECT NO.<br>RR 011-07-41-4807<br>c.<br>RR 022-01-46-5430<br>d. | 9a. ORIGINATOR'S REPORT NUMBER(S)<br>NRL Report 7498<br>9b. OTHER REPORT NO(S) *(Any other numbers that may be assigned this report)* | |

10. DISTRIBUTION STATEMENT
Approved for public release; distribution unlimited.

| | |
|---|---|
| 11. SUPPLEMENTARY NOTES | 12. SPONSORING MILITARY ACTIVITY<br>Department of the Navy<br>Office of Naval Research<br>Arlington, Virginia 22217 |

13. ABSTRACT

Holography, with its unique depth of field and interferometric capabilities, is a powerful new tool for the study of crystal growth. This report describes the theory and practice of forming and reconstructing holograms as applied to the study of microscopic phenomena. It outlines the technical considerations involved in the design of a holographic laboratory and describes the type of experimental results which may be obtained. A holographic laboratory could employ several techniques of holographic microscopy, including holographic interferometry. In the holographic work at NRL an argon ion laser was used to record holograms of transparent organic analogs to solidifying metals. Special observation chambers were constructed to allow holographic recording of planar solid/liquid interfaces, dendrites, floating crystals, and liquid inclusions in crystals. Crystal morphologies were measured by interferometric analysis of the reconstructed holograms. Crystal imperfections were shown to initiate surface relief features. A 2-percent anisotropy of the solid/liquid surface energy was found to control anisotropic crystal growth.

DD FORM 1 NOV 65 1473 (PAGE 1)

S/N 0101-807-6801



Security Classification

Security Classification

| 14. KEY WORDS | LINK A | | LINK B | | LINK C | |
|---|---|---|---|---|---|---|
| | ROLE | WT | ROLE | WT | ROLE | WT |
| Holography | | | | | | |
| Interferometry | | | | | | |
| Microscopy | | | | | | |
| Crystal growth | | | | | | |
| Surface energy | | | | | | |
| Dendrites | | | | | | |
| Metal solidification | | | | | | |

DD FORM 1 NOV 65 1473 (BACK)
(PAGE 2)



Security Classification